PHOTOCATALYTIC OXIDATION OF NO_X OVER TiO_2 CONTAINING CEMENT BASED MATERIALS

A THESIS SUBMITTED TO
THE GRADUATE SCHOOL OF NATURAL AND APPLIED SCIENCES
OF
MIDDLE EAST TECHNICAL UNIVERSITY

BY

IBRAHIM BAYAR

IN PARTIAL FULFILLMENT OF THE REQUIREMENTS
FOR
THE DEGREE OF MASTER OF SCIENCE
IN
CHEMICAL ENGINEERING

AUGUST 2013

Approval of thesis:

PHOTOCATALYTIC OXIDATION OF NO_X OVER TiO_2 CONTAINING CEMENT BASED MATERIALS

submitted by **IBRAHIM BAYAR** in partial fulfillment of the requirements for the degree of **Master of Science in Chemical Engineering Department, Middle East Technical University** by,

Prof. Dr. Canan Özgen _____
Dean, Graduate School of **Natural and Applied Sciences**

Prof. Dr. Deniz Üner _____
Head of Department, **Chemical Engineering**

Prof. Dr. Deniz Üner _____
Supervisor, **Chemical Engineering Dept., METU**

Examining Committee Members:

Prof. Dr. Hayrettin Yücel _____
Chemical Engineering Dept., METU

Prof. Dr. Deniz Üner _____
Chemical Engineering Dept., METU

Asst. Prof. Dr. Emrah Özensoy _____
Chemistry Dept., Bilkent University

Asst. Prof. Dr. Serkan Kıncal _____
Chemical Engineering Dept., METU

Prof. Dr. Oğuz Gülseren _____
Physics Dept., Bilkent University

Date: _____

I hereby declare that all information in this document has been obtained and presented in accordance with academic rules and ethical conduct. I also declare that, as required by these rules and conduct, I have fully cited and referenced all material and results that are not original to this work.

Name, Last name: Ibrahim BAYAR

Signature :

ABSTRACT

PHOTOCATALYTIC OXIDATION OF NO_X OVER TiO_2 CONTAINING CEMENT BASED MATERIALS

Ibrahim, Bayar
M. Sc. Department of Chemical Engineering
Supervisor: Prof. Dr. Deniz Üner

August 2013, 84 pages

The scope of this thesis was to construct a NO_X analysis test system based on ISO-22197:2007(E) standard that can monitor NO oxidation ability of photocatalytically active surfaces. The activity of cement based materials containing TiO_2 on photocatalytic oxidation of NO_X was observed in this test system. In addition, the experimental validity of the ISO-22197:2007(E) standard was verified. Improvements and modifications are recommended. The method was tested on TiO_2 samples coated on the glass, coated on the grout and prepared in the grout samples. Doctor blade method and sol-gel method was used on the glass coating. Experiments indicated that TiO_2 on the surface of the grout exhibits more catalytic activity in oxidation of NO than the same amount of TiO_2 in the grout. The reaction order on TiO_2 with respect to NO concentration is determined to be positive. Evidence was collected for photo-assisted NO adsorption on the surface of the sample.

Cement-bound photo-catalysts are especially attractive for large-scale applications, because cement is a relatively low cost binder. TiO_2 is widely used for the application to the improvement of the living environment due to anti-stain, self-cleaning, and super hydrophilic properties. It can be used simultaneously as a structural component and photocatalytically active material. NO oxidation is a diagnostic tool for photocatalytic activity. Standard methods are necessary to analyze the activity of photocatalytic materials on NO_x oxidation. But, the only standard method validated to analyze photocatalytic activity is ISO-22197:2007(E) standard.

In the experimental part, the effects of relative humidity, catalyst loading, inlet concentration of pollutant and total flow rate of inlet gas on NO oxidation rates were analyzed. In addition, photocatalytic the activity of some industrial samples for oxidation of NO_X is investigated. The activity of the sample is improved with increasing TiO_2 amounts. Photo-assisted adsorption of the NO on the surface of the sample was also observed. Experiments performed in dark indicated that UV irradiation created active sites over TiO_2 for adsorption of NO. Water adsorption calorimetry studies indicated that TiO_2 surfaces can easily adsorb water, with a heat of adsorption of 80 kJ/mol in the first monolayer. On the contrary oxygen adsorption is not as facile as water adsorption.

Keywords: Photocatalytic, Oxidation, Cement, TiO_2, NO_X, Self-cleaning

ÖZ

ÇİMENTO ESASLI MALZEMELERİ İÇEREN TiO_2 İLE NO_X'UN FOTOKATALİTİK OKSİTLENMESİ

Ibrahim, Bayar
Yüksek Lisans, Kimya Mühendisliği Bölümü
Tez Yöneticisi: Prof. Dr. Deniz Üner

Ağustos 2013, 84 sayfa

Bu tezin amacı, fotokatalitik olarak aktif yüzeylerin NO oksitlenmesini gözlemleyen ISO-22197:2007(E) standardını temel alan NO_X analiz sistemini kurmaktır. TiO_2 içeren çimento esaslı malzemelerin fotokatalitik NO_X oksitlenmesindeki aktivitesi test sisteminde gözlemlendi. Buna ek olarak, ISO-22197:2007(E) standardının deneysel geçerliliği ispatlandı. Geliştirmeler ve iyileştirmeler önerildi. Bu metot, cam, harç üzerinde kaplanmış ve harç örnekleri içinde hazırlanmış TiO_2 örneklerinde test edildi. Doktor bıçağı metodu ve sol-jel metodu, cam kaplamada kullanıldı. Deneyler, fotokatalitik NO oksitlenmesinde harç üstüne kaplanan TiO_2'in harç içindeki TiO_2'den daha fazla katalitik aktivite ortaya koyduğunu gösterdi. TiO_2 üzerindeki reaksiyon basamağının NO konsantrasyonuna göre pozitif olduğu belirlendi. Örnek yüzeyindeki ışık destekli NO emilimi için kanıtlar toplandı.

Çimento içindeki fotokatalizörler, çimento bağlayıcıların göreceli düşük maliyetinden dolayı büyük ölçekli uygulamalarda özellikle caziptir. TiO_2 genellikle leke karşıtı, kendi kendini temizleme ve super hidrofilik özelliklerinden dolayı içinde yaşanan çevrenin geliştirilmesi uygulamaları için kullanılır. Aynı anda, fotokatalitik olarak aktif malzeme ve yapısal bileşen olarak hizmet eder. NO oksitlenmesi, fotokatalitik aktivite için bir tanı aracıdır. NO oksitlenmesinde, fotokatalitik malzemelerin aktivitesini analiz etmek için standart metotlar gereklidir. Ama, ISO-22197:2007(E) standardı fotokatalitik aktivite analizi için geçerli tek standart metottur.

Deneysel bölümde, bağıl nemin, katalizör miktarının, kirletici maddenin giriş konsantrasyonunun ve giriş gazının toplam akış hızının NO oksitlenmesi hızı üzerindeki etkileri incelendi. Ek olarak, bazı sanayi numunelerinin NO_X oksitlenmesindeki fotokatalitik aktiviteleri araştırıldı. Bu deneylerin sonuçları, TiO_2 miktarı arttıkça, numune aktivitesinin iyileştiğini gösterdi. Numune yüzeyinde ışıma altında yüksek NO adsoplanması gerçekleşti. Karanlık ortamda NO miktarının adsorplanmasını gösteren deneyler, UV ışığı altında TiO_2 yüzeyinde NO adsoplayan yeni merkezler oluştuğunu gösterdi. Su adsorplanma kalorimetre çalışmaları, TiO_2 yüzeyinde ilk tekkat adsorplanma tabakasında 80 kJ/mol adsorplanma ısısı ile suyun kolaylıkla adsorplandığını gisterdi. Buna karşılık oksijen adsorplanmasının su adsorplanması kadar kolay olmadığı gözlemlendi.

Anahtar Kelimeler: Fotokatalizör, Oksidasyon, Çimento, TiO_2, NO_X, Kendini Temizleme

To my family

ACKNOWLEDGEMENTS

I would like to express my sincere and deep gratitude to my supervisor Prof. Dr. Deniz Uner for her constant support, guidance, valuable kindness and patience. She always motivated and encouraged me towards research. Her great knowledge base, experience and advice shaped my academic and world views greatly. It was a great honor to work with her.

I also want to thank all members, present and former, of CACTUS Research Group. Their ideas and help always shed light on this study. I particularly wish to express my gratefulness to: Atalay Calısan. Nevzat Can Aksu, Necip Berker Uner, Mustafa Yasin Aslan, Cihan Ates, Arzu Kanca, Mert Mehmet Oymak, and Hale Ay.

I would like to thank the following for their feedback and inspiration on this work and in my life: Celal Guvenc Ogulgonen, Gokhan Celik, Okan Ozkok, Onur Erdem, Cemre Avsar, Hasan Zerze, Tarık Yucel, Burcu Gokbudak. The technical staff of our department Süleyman Nazif Kuşhan, Ertuğrul Özdemir, Adil Demir and İsa Çağlar were greatly appreciated for their expertise and help.

My family has provided endless support during my life; Emine Bayar, Mahmut Bayar, Celal Bayar, Ali Bayar and Hatice Bayar. I express many thanks to my cousin Ibrahim Bayar for his contributions to my life. I am also thankful for all the love, support, patience and confidence by Damla Uygar Irs. I am very proud of being a member of Bayar and Gul family. My three cousins, Gülay Bayar, Kazım Gul, Necmettin Tacyildiz my uncle Ahmet Bayar and my grandmother Hatice Gul were not able to see this work completed. Their memories were always with me all the way to the end.

Last but not the least, SANTEZ-00336.STZ.2008-2 and Kalekim A.S. are kindly acknowledged for scholarship and financial support during a part of my graduate studies.

TABLE OF CONTENTS

APPENDICES

LIST OF TABLES

TABLES

LIST OF FIGURES

FIGURES

CHAPTER 1

INTRODUCTION AND OBJECTIVE

The objective of this thesis was to construct a NO_X analysis test system based on ISO-22197:2007(E) standard that can monitor NO oxidation ability of photocatalytically active surfaces. The test samples were prepared in laboratory or provided by the industry. The experimental system was home-built in the laboratory around Teledyne mass flow controllers and the Model 42i Chemiluminescence NO-NO_2-NO_X Analyzer (Thermo Fisher Scientific Inc.). This system is used to assess the photocatalytic NO oxidation activity of different applications such as those collected in Table 1. Examples for these applications on many buildings and city roads are presented in Table 2.

Table 1. Some applications of photocatalytic oxidation of NO_x

Applications	Coating	Reference
Commercial paints	Spread over the surface of the glass panels (a. Mineral silicate paint treated with 10% TiO_2 b. water-based styrene acrylic paint treated with TiO_2)	[1]
The surface of panels on the walls of an artificial 20 m canyon street	Spread over the surface of panels (TiO_2 on the surface of mix mortar)	[2]
Active paving blocks	Surface of pavement blocks	[3], [4]
Air purification panels	a photocatalyst-containing cement coating	[5]
The water permeable paved road surface	Top coated with a mixture containing TiO_2 photocatalyst, water, and additives	[6]
Sound-proof walls on a road or highway	Photocatalytic materials are applied on the sound-proof walls	[7], [8]
A photocatalyst-impregnated cement compound	a photocatalyst-containing cement layer having a thickness of 0.3-2 mm	[9]

Table 2. Examples for applications [10]

Area	City	Country
Church 'Dives in Misericordia'	Rome	Italy
An exterior wall of the Central St. Martins College of Art and Design	Camden	United Kingdom
Air France Building	Roissy-Charles de Gaulle Airport	France
Urban Surfaces (50 000 m^2)	-	Japan
Several city sidewalks and roads		Italy
A parking area	Antwerp	Belgium
Police Central Station	Bordeaux	France
Metro Station	Manila	Philippines
Saint John's Court	Montacarlo	Monaco
Highway wall panels	Tokyo	Japan
A children playground	London	United Kingdom
Music and Arts City Hall	Chambery	France

Scientific studies about photocatalysis have started with TiO_2 in the early part of the 20th century [11]. On the other hand, TiO_2 has been used since ancient times as white pigment. The first known study about photoactivity of TiO_2 is photo bleaching of dyes by TiO_2 both *in vacuo* and in oxygen in1938 [11]. Photocatalysis by using TiO_2 gained the main importance in 1972 after A. Fujishima and K. Honda [12], study about photocatalytic splitting of water on TiO_2 electrodes.

TiO_2 is very commonly used photocatalyst for many reasons. It fulfills the following requirements for efficient photo activity under solar radiation; TiO_2 is strong oxidizing power, at ambient temperature and pressure; band gap of solid state (3.0 eV for rutile and 3.2 eV for anatase) enables it to be useful in the ultraviolet (λ<380 nm) region of the spectrum; superoxide from dioxygen is produced by photo-generated electrons; it has depolluting, self-cleaning, anti-bacterial properties; it is chemically inert, non-toxic, super hydrophilic, cheap and readily available; it has physical stability; it is stable in the presence of aqueous electrolyte solutions.

Titanium is the ninth most abundant element and the fourth most abundant metal in the world, exceeded only by aluminum, magnesium and iron. Titanium (IV) oxide occurs in nature in three crystalline forms; rutile and anatase (tetragonal form) and brookite (rhombic form) [13].

Table 3. Some bulk and thermodynamics properties of the three main polymorphs of TiO_2

Form	Crystal System[14]	Density (g/cm^3)[14]	Band gap (eV)[15]	$\Delta_f G°$[16] (kJ/mol)	$\Delta_f H°$[17] (kJ/mol)
Anatase	Tetragonal	3.83	~3.2	-828.192	-951.345
Rutile	Tetragonal	4.24	~3.0	-837.833	-951.634
Brookite	Rhombohedral	4.17	~3.3	-	-

These are originally pure while they can contain some impurities such as iron and vanadium. TiO_2 has different photocatalytic properties with respect to crystalline type. Anatase and rutile forms are mostly used commercially. On the other hand, brookite is not commercially available, and must be carefully synthesized in the laboratory. The scientific studies generally focus on the anatase phase due to their higher activity [13,18]. In addition, anatase has 0.1 eV higher Fermi level than rutile.

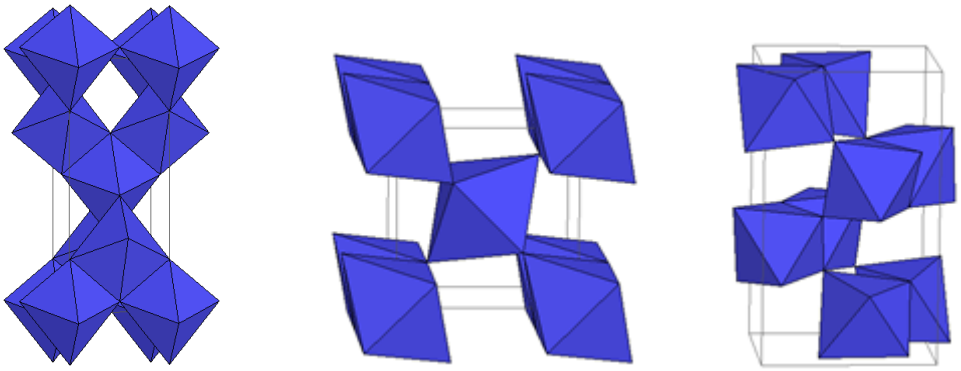

(a) (b) (c)

Figure 1. Three main crystalline forms of TiO_2 (a) anatase, (b) rutile, and (c) brookite [14]

TiO_2 additives are becoming popular for cement based materials. Portland cement is the main binding material for concrete. It is used as construction material. Cement-bound photo-catalysts are especially attractive for large-scale applications, because cement is a relatively low cost binder. It can be used simultaneously as a photocatalytically active material and a structural component.

1.1 Photocatalysis on TiO_2 Surfaces

Titanium was discovered in 1791 in Cornwall, England by Reverend William Gregor. Several years later, it was named by Martin Heinrich Klaport who was German chemist. After Fujishima and Honda's study about photocatalytic splitting of water on TiO_2 electrodes in 1972, a lot of research has been performed by physicists, chemists and chemical engineers. The focus is mostly on the pollutant removal and energy storage [12]. In the 1980s, photocatalytic H_2 production received the main attention. By the 1990s, photocatalysis and hydrophilicity of TiO_2 gained more popularity and TiO_2 has become a part of real industrial applications [11].

The surface of the TiO_2 has become a very popular research area for many scientists due to wide range of its applications and expectation from improving materials and device performance by TiO_2. Hoffmann et al. [19] stated that TiO_2 has been applied to a very large area; water and air purification, the fixation of nitrogen, the inactivation of cancer cells, the clean-up of oil spills, destruction of microorganisms such as viruses and bacteria, the photo splitting of water to produce hydrogen gas and odor control.

1.2 Principle of Heterogeneous Photocatalysis

Photon activation of a semiconductor plays the major role in the heterogeneous photocatalysis. When semiconducting material is photo irradiated with light energy consisting of wavelengths shorter than its band gap, photocatalysis reactions start with photoexcited electrons (e^-) in the conduction band. At the same time, positive holes (h^+) are generated in the valence band. So, electron-hole pairs are generated such that electrons at edge of the conduction band act as reduction centers while the holes at the valance band act as oxidizing sites.

The change on the chemical structure of TiO_2 with characteristic times and the redox processes occurring at the active TiO_2 sites are shown in Figure 2. After the electron-hole pair generation, the radical ions take a part in the process. Charge is carried in different forms. Reaction of holes in the valance band (h^+) with surface titanol groups ($>Ti^{IV}OH$) can

form $\{>Ti^{IV}OH\bullet\}^+$ charge-carrier[1]. Formation of conductance band electron can transform ($>Ti^{IV}OH$) to ($>Ti^{III}OH$). In addition, it can reduce ($>Ti^{IV}$) to ($>Ti^{III}$) irreversibly.

The electron-hole recombination on the surface and in the bulk may occur due to the slowed-down outward diffusion or hydrophobicity [14]. Back electron-transfer reactions convert $\{>Ti^{IV}OH\bullet\}^+$ and ($>Ti^{III}OH$) to ($>Ti^{IV}OH$).

In the degradation process, $\{>Ti^{IV}OH\bullet\}^+$ and ($>Ti^{III}OH$) may move to the surface. They can play a main role in chemical reactions. Organic compounds can give electron to $\{>Ti^{IV}OH\bullet\}^+$ by forming ($>Ti^{IV}OH$). At the same time, the photo-generated electrons produce superoxide (O_2^-). Otherwise, charge would build up [14].

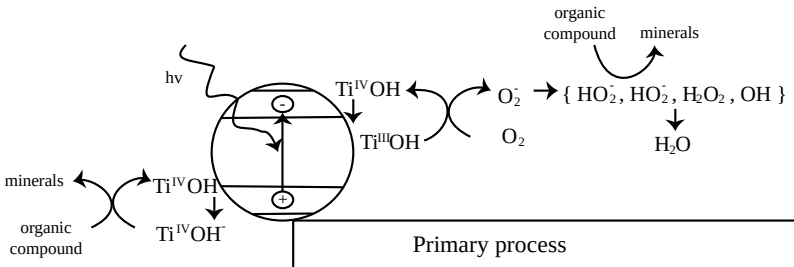

Primary process	Characteristic times
1. Charge-carrier generation:	
$TiO_2 + hv \rightarrow e^-_{CB} + h^+_{VB}$	fast
2. Charge-carrier trapping:	
a. $h^+_{VB} + >Ti^{IV}OH \rightarrow \{>Ti^{IV}OH\bullet\}^+$	fast (10 ns)
b. $e^-_{CB} + >Ti^{IV}OH \leftrightarrow \{>Ti^{III}OH\}$	
(shallow traps, dynamic equilibrium)	(100 ps)
c. $e^-_{CB} + >Ti^{IV} \rightarrow >Ti^{III}$	(10 ns)
(deep traps, irreversible)	
3. Surface charge-carrier recombination:	
a. $e^-_{CB} + \{>Ti^{IV}OH\bullet\}^+ \rightarrow >Ti^{IV}OH$	slow (100 ns)
b. $h^+_{VB} + \{>Ti^{III}OH\} \rightarrow >Ti^{IV}OH$	fast (10 ns)
4. Interfacial charge transfer:	
a. $\{>Ti^{IV}OH\bullet\}^+ + Red \rightarrow >Ti^{IV}OH + Red\bullet^+$	slow (100 ns)
b. $e^-_{CB} + Ox \rightarrow >Ti^{IV}OH + Ox\bullet^-$	very slow (ms)

Figure 2. The change on the chemical structure of TiO_2 with characteristic times and the redox processes occurring at the active TiO_2 sites for TiO_2 -sensitized photooxidative mineralization of organic compounds [14]

[1] The symbol ">" refers to surface of the TiO_2.

Five independent steps can summarize the overall process; i) Reactants are transferred from the fluid phase to the surface, ii) at least one of the reactants are adsorbed on the surface, iii) The occurrence of reaction in the adsorbed phase, iv) Products are desorbed, v) Products are removed from the interface region [18].

1.3 NO_x Oxidation

Chemical industry is the central to the world economy and has a huge impact on environment. Harmful gas emissions such as NO_x and SO_x gases formed during combustion processes in industry is the main source of this impact. NO_x is also one of the pollutant gases in exhaust emissions from vehicles. Briefly, all combustion processes are sources of NO_x[2]. Most of NO_x is emitted as NO. There are various environmental problems caused by NO_x; such as acid rains and photochemical smog. Heterogeneous photocatalysis is the attractive way to destruction of NO_x. EPA Technical Bulletin [20] showed that, among the anthropogenic sources, approximately 50% of the NO_x emissions comes from mobile sources; 20% of the NO_x emissions comes from electric power plants; 30% of the NO_x emissions comes from everything else. Everything else contains such as cement manufacture, biogenic or natural sources of nitrogen oxides, iron and steel mills, glass manufacture. According to Environmental Protection Agency, the group of NO_x compounds with their properties is shown in Table 4.

NO_x emission is controlled by two approaches. One of them is the reduction of NO_x back to N_2. The other approach is the oxidation of NO_X to NO_2 and HNO_3. The second way is a good example to convert pollutant into a product such as fertilizer.

Under UV light irradiation, wavelengths less than 380 nm, TiO_2 is activated to induce some chemical reactions such as oxidation of NO_x. This photocatalysis process occurs as i) TiO_2 has electron hole pair under UV light, electron and hole trapping, ii) NO_x is oxidized by using hydroxyl radicals (OH●) , iii) active oxygen (O_2^-) also oxidizes NO_x, iv) reaction with Ti-OH via disproportionation is occurred, v) [HNO_3] complex is removed from the catalyst surface by water [21].

[2] NO_x represents N_2O, NO and NO_2 compounds.

Table 4. Nitrogen Oxides (NO_x) [20]

Formula	Name	Nitrogen Valance	Properties	$\Delta_f H°$ (kJ/mol)[74]	$\Delta_f G°$ (kJ/mol)[74]
N_2O	nitrous oxide	1	colorless gas water soluble	81.6	103.7
NO	nitric oxide	2	colorless gas slightly water soluble	91.29	87.6
N_2O_3	dinitrogen trioxide	3	black solid water soluble, decomposes in water	86.8 (g)	142.4 (g)
NO_2	nitrogen dioxide	4	red-brown gas very water soluble, decomposes in water	33.1	51.3
N_2O_4	dinitrogen tetroxide	4	red-brown gas very water soluble, decomposes in water	11.1	99.8
N_2O_5	dinitrogen pentoxide	5	white solid very water soluble, decomposes in water	11.3 (g)	117.1 (g)

1.4 ISO-22197:2007(E) Standard (Part 1: Removal of Nitric Oxide)

This ISO standard contains a test method which helps to analyze the activity of the photocatalytic materials such as titanium dioxide or other ceramic materials on the air purification performance. This standard determines the principle of the test method, apparatus used in this test, test piece, procedure and evaluation of the results. This method only concerns removal of nitric oxide besides of the determination of other performance attributes of photocatalytic materials such as decomposition of water contaminants, self-cleaning, antifogging and antibacterial actions [22].

The principle of this ISO Standard is the development, comparison, quality assurance, characterization, reliability, and the design data generation of photocatalytic materials. The activity of test material is determined by finding the amount of the net removed nitrogen oxides [22].

1.5 Objectives and Outline of the Thesis

The motivation of this thesis was to construct a NO_X analysis test system based on ISO-22197:2007(E) standard that can monitor NO oxidation ability of photocatalytically active surfaces. In this thesis, heterogeneous photocatalysis, applications, photocatalysis on TiO_2, NO_x oxidation and ISO-22197:2007(E) Standard were briefly introduced in Chapter 1. Then, a literature survey based on surface science of TiO_2, photocatalytic activity of TiO_2 and effective parameters on this activity , NO_X abatement, reaction mechanisms on the surface of TiO_2 for photocatalytic oxidation of NO_X, catalyst preparation as a thin film, water denitrification were presented in Chapter 2. Materials and methods used in this study were explained in Chapter 3. All of the results obtained in the fundemental experiments were discussed in detail in Chapter 4. The whole study in this thesis was summarized in Chapter 5.

CHAPTER 2

LITERATURE SURVEY

2.1 Heterogeneous Photocatalysis

Heterogeneous photocatalysis includes a large variety of reactions. It is thought as one of the new 'advanced oxidation technologies' AOT for air and water purification treatment [18]. More than 1200 references were reported on this subject by 1999 [23]. There are three major review articles that give the most detailed account of the surface science of TiO_2 and photocatalysis on TiO_2 surfaces: Linsebigler et al. [12], Carp et al. [14] and Diebold [24].

Linsebigler et al. [12] reported principles, mechanisms and selected results about photocatalysis on TiO_2 surfaces up to 1995. The scope of this review article was to give a detailed description of the energy transfer and electron transfer processes in photocatalytic reactions. There are four sections in this review article. So, they summarized some of the operating principles of heterogeneous photocatalysis and focused on the interfacial processes in the first section. Catalyzed and sensitized photoreactions were discussed by looking at the electronic excitation processes in section 2. The processes occur in a semiconductor and a molecule substrate. In section 3, the fundamental principles and common characteristics of the TiO_2-based photocatalysis systems were summarized by comparing thermal and photocatalytic studies on TiO_2. The basic idea in section 4 was to give research efforts in the semiconductor catalysts with the electronic modification.

In the first section, they gave an introduction to heterogeneous photocatalysis systems. They classified the photocatalysis processes into two classes based on where the initial excitation occurs. The first process is catalyzed photoreaction. An adsorbate molecule is the place where the initial excitation takes in. Then, it interacts with the ground state catalyst substrate. The second process is called as a sensitized photoreaction. The catalyst substrate is the place where the initial excitation occurs. An electron or energy is transferred from the photoexcited catalyst into a ground state molecule. After initial excitation, deexcitation process follows the heterogeneous photocatalysis process. It leads chemical reactions by electron or energy transfer [12].

In section 2, the efficiency of the photoinduced chemistry is analyzed. The control of the efficiency depends on the system's light absorption characteristics. The light absorption

intensity is changed according to interfacial electron transfer, the band-gap excitation of the semiconductor substrate and the electronic excitation of a molecule upon photon absorption [12].

In section 3, the lattice and electronic structure of TiO_2 is explained for anatase and rutile crystal structures. The anatase shows a higher photocatalytic activity.TiO_2 (110) surface is thermodynamically most stable. In addition, results of chemisorption studies on TiO_2 surfaces are summarized. Water, H_2, oxygen, CO and CO_2, NO and SO_2, NH_3 and H_2S adsorptions are investigated. In this review, surface hydroxyl groups were detected after H_2O adsorption at 300 K on a slightly defective TiO_2 (110) surface. It is indicated that the coverage of oxygen vacancy defect sites does not affect the coverage of OH. It is found that water adsorption is intact below 160 K, while water produces hydroxyl groups above 200 K. Ti^{3+} sites on the TiO_2(110) surface can reduce water molecules to produce hydrogen gas. After these chemisorption studies, photooxidation on TiO_2 single crystals is reported. Single-crystal surfaces are used to study three different subjects. These are the surface reactive sites, controlled surface coverages of the reactant molecules and a well-ordered structure with known surface area. Studies about photooxidation at the gas-solid and liquid-solid interface on TiO_2 catalysts are gathered together. The related part with this study is the effects of adsorbed H_2O and O_2 on the photoactivity of TiO_2. They made a conclusion as an effective electron-hole recombination center can be the adsorbed water. On the other hand, an effective electron trap can be the adsorbed oxygen. It prevents a recombination process [12].

Finally, surface modifications are determined to develop the activity of the semiconductor particles. Three strategies to modify photocatalytic semiconductor systems are applied to overlap the limitations of a photocatalyst. One of them is that the charge separation can be increased to inhibit recombination, so the efficiency is higher for the photocatalytic process. The second one is that the wavelength response range can be increased. The third one is that the yield or selectivity of a particular product can be changed [12].

Diebold [24] prepared a comprehensive review of the surface science of TiO_2 by focusing on the publications after 1990. She explained that TiO_2 has been taken as the model system in the surface science of metal oxides for many reasons. One of them is that it is well-suited for many experimental techniques. The others are that it is easily reduced and polished crystals with a high surface quality can be obtained. Her main motivation is to contribute to the knowledge of surface science of metal oxides [24].

Diebold shows the importance of TiO_2 by pointing to its applications. It can be used in heterogeneous catalysis, electric devices, solar cells magnetic spin-valve systems, the biocompatibility of bone implants and ceramics. Surface investigation on TiO_2 is one main driving force to understand and improve catalytic reactions. There are four sections in this review article to understand surface of TiO_2. The geometric structure of various TiO_2 surface is explained in section 1. The electronic structure of TiO_2 is mentioned in section 2. The development of metal and metal oxide on the surface of TiO_2 substrates is reported in section 3. Finally, section 4 contains the surface chemistry of TiO_2 [24].

In the first part, the surface structure of TiO_2 system was discussed. There are two opposite opinions in the survey. One of them is simple approaches explain surface structure very well. The opposite lesson is that oxide surfaces are difficult to understand. It is concluded that the rutile TiO_2 among metal oxides is very popular model system due to the expanding data base. It is also expected anatase to get more interest by the recent process [24].

In the second part, powerful computational and theoretical approaches to TiO_2 surfaces were used to focus on the vibrational and electronic structure of TiO_2 surfaces. The popular idea is to know adsorption of molecules and metals by calculations. The third part contains the metal/TiO_2 systems. A lot of elements in Figure 3 have been studied on single-crystalline TiO_2 surfaces [24].

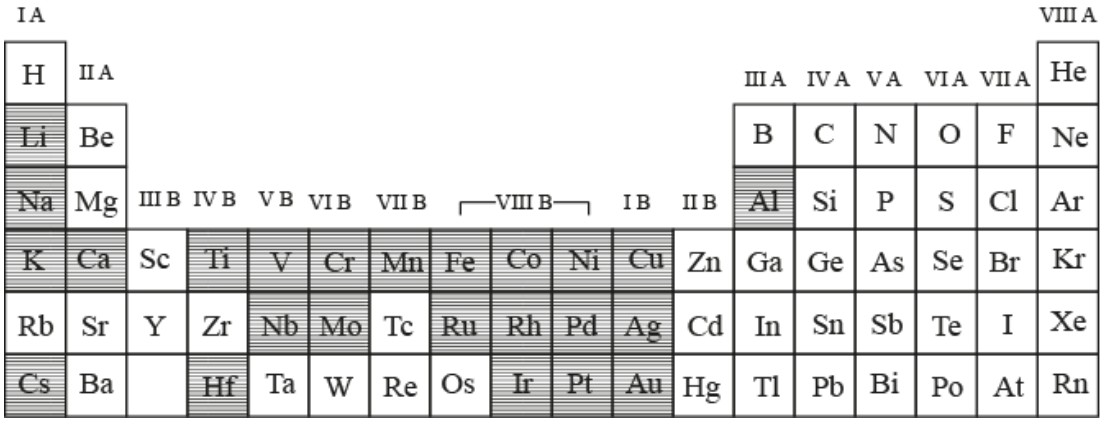

Figure 3. Elements on single-crystalline TiO_2 surfaces have been studied for adsorption and/or growth [24]

The adsorption of molecules and atoms and their dissociation or conversion to other products with respect to the surface chemistry of TiO_2 were discussed in the last part. It is divided to two sections as adsorption of inorganic and organic molecules on TiO_2 which were tabulated in Table 5. Finally, this review article pointed out that surface(s) of TiO_2 are very complicated. It will help to give more fundamental perspectives and various studies on TiO_2.

Table 5. Inorganic and organic molecules adsorbed on TiO_2[24]

Inorganic Molecules	Organic Molecules
Hydrogen	Carboxylic acids
Water	
Oxygen	
Carbon Monoxide and Carbon Dioxide (CO, CO_2)	Alcohols (Methanol, higher alcohols)
Nitrogen-containing molecules (N_2, NO_2, N_2O, NO, NH_3)	Aldehydes and ketones
Sulfur-containing molecules (SO_2, H_2S, elemental sulfur)	Cyclo-trimerization of alkynes
Halogen-containing molecules (HI, Cl_2, CrO_2Cl_2)	STM of pyridine, its derivatives and other aromatic molecules
Rare gases (Ar, Xe)	Silanes

Carp et al. [14] prepared a review article about photoinduced reactivity of titanium dioxide by examining 1370 references up to 2004. This paper aims to give an overview of this field. They classified use of the energy which can be created by excitation of semiconductors by light into three categories. It can be used chemically in photochemical catalysis, electrically in solar cells and to change the catalyst surface itself as superhydrophilicity. Titanium dioxide is investigated among semiconductors in this review. There are three parts in the review article. Introduction to titanium dioxide and its photoinduced processes are mentioned in the first part. Photocatalytic reactions and mechanisms are reported in detail in the second part. In the last part, the research about the application of titanium dioxide as a photoactive material is explained [14].

Titanium dioxide is defined very well in the first part. The production of TiO_2, the major end-use sectors of TiO_2, its crystal structure and properties, its synthesis and morphologies and semiconductors and photocatalytic activity are the basic concepts in this section. The end-use sectors are paints, plastic, paper, textiles, food, leather and pharmaceuticals. The difference between structures of TiO_2 (anatase, rutile and brookite) are the distortion of each octahedral and the assembly patterns of octahedral chains. The rutile is predicted as the most stable phase at all temperatures and pressure up to 60 kbar according to thermodynamic calculations in the light of calorimetric data. But, particle sizes have impacts on the phase stability due to surface stress and surface free energy. Particle size determines them. The three crystalline phases in the same particle sizes were compared. The experiments showed

that the most thermodynamically stable structure was anatase at sizes less than 11 nm, brookite between 11 and 35 nm and rutile at sizes greater than 35 nm. Preparation of TiO_2 in forms of powder, crystals and thin films is presented in Table 6. Liquid phase and gas phase processing are two synthesis routes [14].

Table 6. Preparation of TiO_2 in forms of powder, crystals and thin films [14]

Solution routes	**Gas phase methods**
Sol-gel methods	Spray pyrolysis deposition (SPD)
Solvothermal methods	Physical vapour deposition (PVD)
Preparation (co-) methods	Chemical vapour deposition (CVD)
Microemulsion methods	Dynamic ion beam
Combustion synthesis	Molecular beam epitaxy
Electrochemical synthesis	Sputtering
	Ion implantation

The ability of semiconductors is controlled by the redox potential of the adsorbates and the band energy positions of the semiconductor, so it transfers photoinduced electron to an adsorbed particle. The band gap of several semiconductors and some standard potential of redox couples is shown in Figure 4.

In the second part, photoinduced processes for photovoltaic cells, photocatalysis and photoinduced superhydrophilicity are described in detail. A photoinduced phenomenon is mentioned in the introduction part. The additional information is to that phenomenon in Carp et al.'s review is the enhancing photocatalysis. Adsorption of organic substances on the catalyst surface is better when surface acidity is high and electron traps is deep. They also extend the lifetime of photo-excited electrons and holes. By the way, hydrophilic surface conversion needs low surface acidity and a large quantity of Ti^{3+}. The selection of a semiconductor photocatalyst depends on being able to efficiently catalyze reactions, efficiently activated by sunlight, photocatalytically stable, chemically and biologically inert, easy to produce and use, with no risks for the humans or environment and cheap. So, TiO_2 can be thought as an ideal photocatalyst except not absorbing visible light. Anatase structure is more photocatalytically active than rutile structure, because Fermi level of anatase is slightly higher, it has higher degree of hydroxylation and lower oxygen adsorption capacity. Photocatalysis processes around TiO_2 are photocatalytic synthetic processes and partial or

total photodegradation, photofixation of nitrogen, solar production of hydrogen from water and photoreduction of CO_2 (artificial photosynthesis) [14].

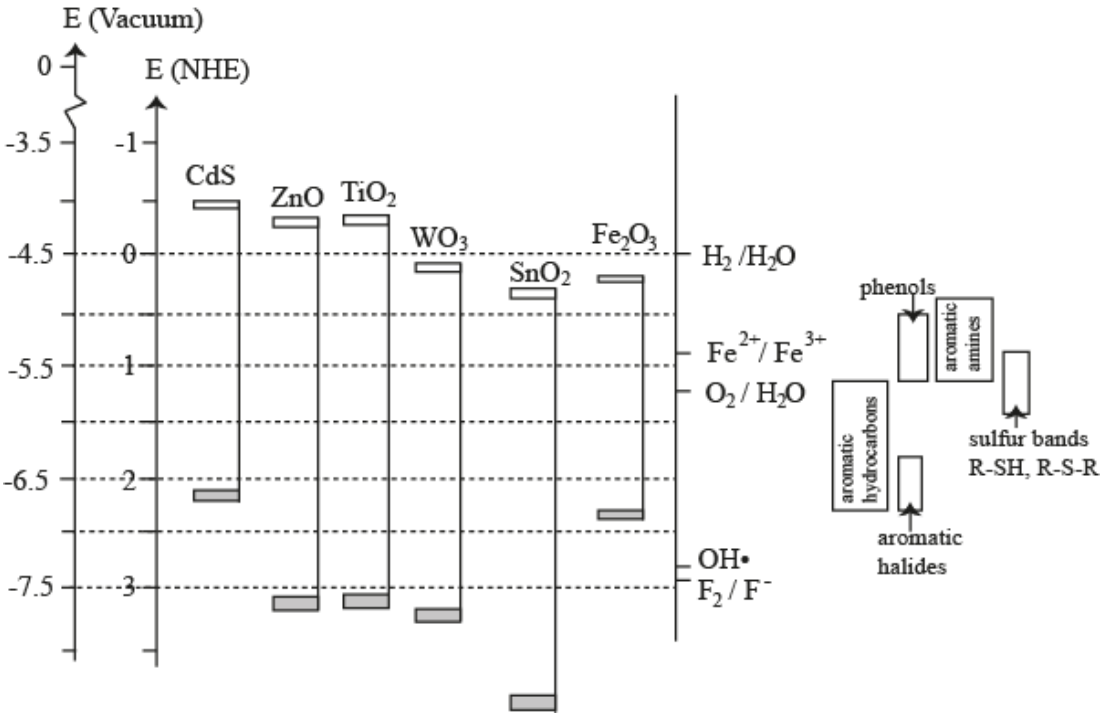

Figure 4. Several semiconductors with band positions (bottom of conduction band and top of valance band) and some selected redox potentials. Picture adapted from [14]

In the second part, photocatalysis are also analyzed according to mechanical aspects. Carp et al. emphasized that mechanism of the photocatalytic process on the TiO_2 surface was not explained in detail clearly up to 2004. Main concern is the initial steps of the reaction of organic molecules and reactive oxygen species. There is an agreement about the rate of the degradation of organic substrates. The Langmuir-Hinshelwood mechanism is applied in the liquid- and gas-phase photocatalysis [14].

The main parameters which affect the degradation rate are determined as oxygen concentration, temperature, UV light intensity, coexisting compound, catalyst dosage, presence of supplementary substance which is oxidizable, character of target compounds, initial concentration of oxidized compound, pH for aqueous treatments, circulating flow rate and water concentration for photoreactions in gas phase. Photodegradation efficiency is expressed in terms of quantum yields, electrical energy per mass or per order and turnover number [14].

In the third part, improving photocatalytic reactions and photocatalytic applications follow the first and second parts. Photocatalytic applications are listed in Table 7. Two approaches are accepted for a photocatalyst system to improving photocatalytic reactions;

1. Catalyst synthesis can be optimized, so catalysts can be with a defined crystal structure and smaller particle sizes. They can also be used for various support materials and metal dopants.
2. TiO_2 catalyst can be designed and developed for second generation to obtain high selectivities. The aim is to use it under solar or visible irradiation effectively.

In conclusion, there is a dilemma between eliminating contaminated compounds and its costs as energy and CO_2 emission. This review article presents semiconductor chemistry as a solution of the dilemma by the use of an inert catalyst (environmentally friendly), solar energy input and non-hazardous oxidants such as oxygen. There is a very rich literature on this subject. There is a need an interdisciplinary effort for detailed investigations. The studies in this subject are that synthesizing TiO_2 photocatalysts, investigation of the structure, morphology and other physical-chemical properties, working on photochemistry which includes theoretical calculations, the importance of the surface and the explanation of reaction mechanism, investigation of practical applications which includes the testing and manufacture of various reactants, reactors and photocatalysts and improvement of the photocatalytic activity [14].

But, there is a disagreement on reaction mechanism, although there is a common point on the importance of OH radicals and the first steps of the reaction. They also reported that one of the biggest problems in this field is comparison between articles due to differences in used photocatalyst and reaction parameters such as concentration of substrates, catalyst loading, light, reaction time and type and reactor set-up. Therefore, there are no general trends in this subject. Finally, the main study for the future focuses the development of a photocatalyst system [14].

Jean-Marie Hermann [18] explained the overall process of heterogeneous photocatalysis. The main difference between conventional catalysis and photocatalysts is the mode of activation of catalyst. In other words, photon activation replace with thermal activation. In addition, Hermann [18] described the effects of the main parameters controlling the kinetics as initial concentration, wavelength, catalyst loading, reaction temperature and radiant flux. Hermann [18] indicated that anatase has higher surface area and the surface density of active sites for adsorption is higher than other allotropic forms of TiO_2 at lower temperature (<600 K).

It is indicated that Titania has the best photocatalytic performance among various chalcogenides (oxide and sulfide), TiO_2, ZnO, CeO_2, CdS, ZnS [12]. Hoffmann et al. [19] also determined that TiO_2 is the most suitable photocatalysts for widespread environmental applications among several simple oxide and sulfide semiconductors. Harada et al. [25] showed that the photocatalytic activity of TiO_2 depends on the crystal structure, porosity, size distribution, surface area, surface hydroxyl group density, etc. [25]. Furthermore, anatase phase is reported as the most active allotropic form in many studies [11,12,13,18]. The differences in the surface hydroxyl groups in the low temperature and Fermi level of anatase phase are determined as the reason of more activity of anatase phase in Aaron's review [13]. In addition, Aaron [13] explained using anatase TiO_2 as an ideal photocatalyst by thermodynamic considerations.

Table 7. Photocatalytic applications [14]

Selective Organic Synthesis	Water Purification				Air Cleaning		Disinfection and anti-tumoral activity
	Combined Process	Organic Compounds	Inorganic compounds		Organic Compounds	Inorganic Compounds	Pathogenic organisms
			Reduction of metal ions	Oxidation of inorganic anions			
Alkanes and Alkenes	TiO_2/bacterial or fungal degradation	Carboxylic acids	Chromium(VI)	Cyanide	Hydrocarbons	Fixation of nitrogen oxides	Gram-negative bacteria
Saturated and unsaturated alicyclic hydrocarbons		Benzoic acid, phenol and their derivates	Nickel(II)		Chlorinated compounds		Gram-positive bacteria
Sulfides		Chlorine-containing compounds	Copper(II)		Alcohols		Viruses
Aromatic compounds		Nitrogen-containing compounds	Ag(I)		Nitrogen-containing compounds		Fungi
Aldehydes, ketones, acids	TiO_2/inorganic oxidants	Sulfur-containing compounds	Hg(II)	Nitrite anions	Sulfur-containing compounds	Ozone	Protozoa
Amines		Selenium-containing compounds	Platinum(II)		Siloxane compounds		Algae
Nitro and nitrous compounds		Humic acids, Surfactants, Pesticides	Lead(II)				Enzyme
Alcohols		Cyanobacterial metabolites					Cancer cells
		Oil derivatives, Dyes					

2.2 Removal of NO_X

It is considered that NO_x is the primary pollutants of the atmosphere. It is responsible for health problems in humans, global warming, acid rain, photochemical smog, ozone layer depletion and tropospheric ozone [26]. The oldest NO_x formation model is the ammonia oxidation. The detailed information about ammonia oxidation and its reaction mechanism is given in Appendix B. NO_x formation is sourced by three combustion types; thermal NO_x, fuel NO_x, and prompt NO_x according to EPA Technical Bulletin [20]. According to same bulletin, the NO_x control methods are shown in Table 8.

Table 8. The list of NO_X Control Methods [20]

Abatement or Emission Control Principle or Method	Successful Technologies	Pollution Prevention Method (P2) or Addon Technology (A)
1.Reducing peak temperature	Inject Water or Steam	P2
	Air Staging	P2
	Flue Gas Recirculation (FGR)	P2
	Low Gas Reburning	P2
	Natural Gas Reburning	P2
	Burners Out Of Service (BOOS)	P2
	Reduced Air Preheat	P2
	Less Excess Air (LEA)	P2
	Catalytic Combustion	P2
	Over Fire Air (OFA)	P2
	Combustion Optimization	P2
2.Reducing residence time at peak temperature	Inject Air	P2
	Inject Fuel	P2
	Inject Steam	P2
3.Chemical reduction of NO_x	Low NO_x Burners (LNB)	P2
	Fuel Reburning (FR)	P2
	Selective Non-Catalytic Reduction (SNCR)	A
	Selective Catalytic Reduction (SCR)	A
4. Oxidation of NO_x with subsequent absorption	Non-Thermal Plasma Reactor	A
	Inject Oxidant	A
5. Removal of nitrogen	Ultra-Low Nitrogen Fuel	P2
	Oxygen Instead Of Air	P2
6. Using a sorbent	Sorbent In Ducts	A
	Sorbent In Combustion Chambers	A
7. Combinations of these Methods	All Commercial Products	P2 and A

The principles of methods to reduce NO_x are basically introduced as;

Method 1. Reducing Temperature – This technique avoids the stoichiometric ratio (the ratio of chemicals in the reaction) by reducing combustion temperature with excess of steam, fuel, flue gas or air [20].

Method 2. Reducing Residence time – This technique avoids the large amount of nitrogen from becoming ionized by injection or ignition timing with internal combustion engines at high combustions [20].

Method 3. Chemical reduction of NO_x – A chemically reducing substance for removing oxygen from nitrogen oxides is provided in this technique [20].

Method 4. Oxidation of NO_x with subsequent absorption – The valance of the nitrogen ion for allowing water to absorb it is raised by using a catalyst, injection hydrogen peroxide, injection ozone into the air flow, or creating ozone within the air flow in this technique [20].

Method 5. Removal of nitrogen – This technique removes nitrogen as a reactant. It also uses oxygen in the combustion processes or ultra-low nitrogen content fuel, so it forms less fuel NO_x [20].

Method 6. Sorption, both adsorption and absorption – This technique can remove NO_x and other pollutants like sulfur by injection of sorbents such as ammonia, carbon, aluminum oxide or powdered limestone [20].

Method 7. Combinations of these methods – This technique contains combination of the other six methods to reduce NO_x concentration [20].

NO_x abatement for lean-burn gasoline and diesel engines creates an active area for researchers for last decades. They have focused on the catalytic technologies due to low cost and high efficiency. Conventional three-way catalysts have been widely applied on the gasoline-fueled engines [27,28]. But, it has been found that they are ineffective in the presence of excess oxygen [27]. Three-way catalysts are composed of platinum, rhodium and palladium. They promote oxidation of carbon monoxide and hydrocarbons effectively. In addition, reduction of nitric oxide to nitrogen and oxygen is other promotion. The challenge with effect of the excess oxygen needs to be solved with development of catalyst.

Garin [29] has reviewed heterogeneous catalysis based on three aspects up to 2003. Three aspects are hydrocarbon reforming reactions, three-way catalysis and $DeNO_x$ catalysis. In Garin's review [29], it is indicated that platinum, palladium and rhodium supported on oxides are signed as the most powerful catalysts in NO degradation. A catalyst model for NO_x trap has three major components: a high surface area supporting material such as γ-Al_2O_3; alkali or alkaline earth metals to store NO_x such as barium and noble metals to reduce nitric oxide such as Pt, Pd or Rh. Huang et al. [30] investigated Pt-Rh/TiO_2/Al_2O_3 as a NO_x storage-reduction catalyst using lean-rich cycles and found that it has 90% conversion for NO_x reduction and resists to SO_2 and H_2O. The SCR of NO_x with ammonia is known as a solution of flue gases released by the chemical industry plants and power stations. Ammonia

is used to reduce NO_x to N_2 and it can reduce also NO_x with reacting by oxygen. But these reactions occur selectively and reduction of NO_x is more dominant one. Pietraszek et al. [31] used methane instead of ammonia, because ammonia is expensive, corrosive reducer and pollutant for reduction of NO to N_2 over 0.03 at. %Rh/Al_2O_3, 0.51 at. %Pt/Al_2O_3, and 0.34 at. %Pt at %Rh/Al_2O_3 catalysts. It is reported that NO_x conversion for $Pt/BaO/Al_2O_3$ decreased from 80% to 18%, and for $Pt\text{-}Rh/BaO/Al_2O_3$ reduced from 99% to 30% in the presence of SO_2.

2.3 Photocatalytic Oxidation of NO_x Over TiO_2 Based Photocatalysts

Skalska et al. [26] added the photocatalytic oxidation of NO_x to these control methods as an alternative NO_x control technologies. She also made final comment as the suitable method to control specific source of NO_x is based on many factors such as temperature of the flue gas, the source itself, regulations concerning this type of source, presence of other pollutants, amount of NO_x present in the flue gas, composition of NO_x.

Yoneyama et al. [32] firstly reported heterogeneous photocatalytic reactions of nitrogen oxide species on TiO_2 as a photocatalyst in $HClO_4$ solution. It was the start of the investigation of photocatalytic oxidation of NO_x in the literature. In this study, illuminated TiO_2 catalyst was used to determine reactions of NO in the solution by using calorimetry. Hori et al. [33] showed that oxidation of NO_2^- ion to NO_3^- in aqueous suspension of TiO_2 depends on the presence of O_2 under illumination.

Ibusuki et al. [34] reported photodegradation of NO_X in the ambient atmosphere via TiO_2 as the photocatalyst. This study differs for previous studies made by Yoneyama et al. and Hori et al. by dry deposition of NO_x. It was stated that TiO_2 powder showed excellent photocatalytic activity for removal of NO by converting to NO_2 and HNO_3. But there was not yet clear explanation for reaction mechanism for photocatalytic reduction of NO_x.

Simonsen et al. [35] investigated the effect of OH groups on the photocatalytic activity of TiO_2 film for steric acid degradation as a model compound. The surface of the thin film was analyzed by XPS. In the light of the experiments, it was suggested that the OH groups on the surface had very high impact on photocatalytic activity of TiO_2. It was also found that the surface properties of the catalyst determine the photocatalytic activity of TiO_2.

Oymak [60] studied on photocatalytic activity in nano sized titanium dioxide structures in cement based materials. He used the commercial TiO_2 powders mixed with grout and plaster in his study. Photocatalytic oxidation activities of these samples were investigated for a potential commercial self cleaning material. NO adsorption studies for 15 different TiO_2 powders showed nitrate and nitrite formations on the surface by interaction with water.

Linsebigler et al. [12] focused on the photocatalysis on TiO_2 surface by chemisorption studies. They searched the effects of adsorbed H_2O and O_2 on photoactivity of TiO_2. Hermann [18] investigated the effects of temperature, catalyst loading, oxygen pressure, wavelength, initial concentration and radiant flux on reaction kinetics for photocatalytic oxidation of NO_x. Dalton et al. [21] made a surface spectroscopic approach on photocatalytic oxidation of NO_x over TiO_2 by using scanning electron microscopy (SEM), Raman spectroscopy and X-ray photoelectron spectroscopy (XPS). Devahasdin et al. [15] determined the effect of inlet concentration/space time, light intensity, relative humidity. Wang et al. [37] also studied on the reaction rate by examining inlet concentration, relative humidity, oxygen percentage and space time. Yin et al. [38] thought that crystallinity and specific surface area is strongly related to photocatalytic activity. They showed that the photocatalytic activity of well-crystallized photocatalysts with a fine particle size is excellent. Yu et al [39] addresses the effective parameters such as irradiance, relative humidity, initial NO concentration, flow rate, photocatalyst dosage. Hüsken et al. [40] presented the research on the parameters that influence the degradation of NO_x such as relative humidity, NO_x concentration, irradiance, flow rate. Hunger et al. [41] investigated the irradiance and relative humidity parameters on degradation of NO_x. In addition, Martinez et al. [42] studied various parameters; the coating composition, relative humidity, the nature of the substrate, the initial concentration of NO and the inlet flow rate. Melo et al. [43] analyzed the influence of flow rate, UV-A radiation, relative humidity on the efficiency of photocatalytic coatings. All these studies are summarized in Table 9.

2.3.1 Relative humidity

This parameter was addressed by many researchers before. All of the researchers accepted that the role of the water is very important in the photocatalytic oxidation of NO. It generates hydroxyl radical in the photocatalyst surface. There are different opinions for the influence of relative humidity on photocatalytic oxidation of NO_X over TiO_2 based catalysts.

Devahasdin et al. [36] reported that the conversion of NO increases from 0 to 50% relative humidity and becomes constant after 50% relative humidity. Tawara et al. [44] found that the conversion of NO increases from 0 to 50% relative humidity and decreases after 50% relative humidity. Tawara and Devahasdin used similar experiment set-ups. But, while inlet concentration was 40 ppm in Devahasdin's study [36], it was 1 ppm in Tawara's study [44]. In addition, the gap between catalyst surface and wall was 5 mm larger in Devahasdin's set-up [36]. Wang et al. [37] reported that the conversion of NO increases when the relative humidity increases from 8 and 60% and the rate is reduced after 60% relative humidity. Yu et al. [39] investigated the change of NO_x conversion varying relative humidity from 10% to 70%. It is found that the conversion increases by increasing relative humidity. Hüsken et al. [40] and Hunger et al. [41] stated that the degradation rate decreases linearly by increasing humidity in the range 10-70% relative humidity range. In Yu's study, the inlet concentration is 0.5 ppm while it is 1 ppm in Hüsken's study. The other parameters were similar. Martinez

et al. [42] reported that there was no change observed on degradation rate of NO, when the inlet concentration of NO was 400 and 1000 ppb. In addition, the degradation rates increases while the humidity increases at higher inlet concentrations (1500 and 2000 ppb). Melo et al. [43] also reported as Hüsken's and Hunger's study that decreases in photocatalytic activity was observed as increasing relative humidity.

Table 9. Investigations on reaction kinetics for photocatalytic oxidation of NO_x

Study	Parameters
Linsebigler et al. [12]	adsorbed H_2O and O_2
Hermann [18]	catalyst loading, oxygen pressure, wavelength, temperature initial concentration and radiant flux
Devahasdin et al. [36]	inlet concentration/space time, light intensity, relative humidity
Wang et al. [37]	relative humidity, inlet concentration, oxygen concentration and space time
Yin et al. [38]	crystallinity and specific surface area
Yu et al [39]	initial pollutant concentration, relative humidity, irradiance, photocatalyst dosage, total flow rate,
Hüsken et al [40]	irradiance, relative humidity, pollutant concentration, flow rate
Hunger et al. [41]	irradiance and relative humidity
Martinez et al. [42]	the coating composition, relative humidity, the nature of the substrate, the initial concentration of NO and the inlet flow rate
Melo et al. [43]	flow rate, UV-A radiation, relative humidity

2.3.2 Catalyst Loading

One of the effective parameters on photocatalytic activity is mass of catalyst. Catalyst loading makes surface area of the catalyst higher for adsorption and degradation. But, there is a certain value for catalyst loading. This optimum value depends on the solution opacity, light scattering property of the particles and the geometry of the photoreactor.

At high concentrations, agglomeration of TiO_2 particles reduces decomposition. Inel et al. [45] reported that the decrease in the surface active sites is resulted by the aggregation of TiO_2 particles at high concentration. Higher catalyst concentration increases opacity by increasing light scattering of the catalyst particles. That leads to a reduction of light penetration through the sample. It means a decrease on the reaction rate. Assabane et al. [46] obtained similar conclusions with Inel's studies about the factors to determine catalyst concentration.

Photoreactors can be chosen based on the reaction as slurry batch photoreactors and fixed bed photoreactors. Chen et al. [47] reported that there is a wide range for different photoreactors and photocatalyzed systems from 0.15 to 8 g/l. They found a big difference in optimum catalyst dosage from 0.15 to 2.5 g/l while the catalyst amount is same for slurry reactors. Carp et el. [14] determined that increasing the thickness of the catalyst film leads to increasing the recombination possibility of the electron/hole pair which decreases the degradation performance in fixed bed reactors. They also pointed that the optical penetration length at certain illumination intensity and catalyst amount should be more than the solution layer thickness for validity of reactor.

There is an opinion about the reaction rate of NO degradation is independent of mass after a certain amount of catalyst. Hermann indicated that initial rates of reaction increase by increasing mass of catalyst until a certain value of mass. Above that value, the reaction rate is constant and independent of mass. Toma et al. [48] and Martinez et al. [42] made the same conclusions in Hermann research about effect of amount of photocatalyst.

The amount of catalyst influences the surface area. Yu et al. [39] and Hüsken et al. [40] emphasized that electron and hole pairs play the major role for the oxidation reaction between adsorbed pollutant and water on the surface. They showed in their studies that increasing of the photocatalyst amount makes the NO_x conversion increases linearly.

2.3.3 Inlet Concentration of Pollutant

Inlet concentration of pollutant also plays an effective role on photocatalytic activity of the photocatalysts. The effectiveness of NO level on the activity took interests due to a wide range of NO levels in the environment. The reaction mechanism of photocatalytic oxidation of NO_x is considered as Langmuir-Hinshelwood mechanism [18,36,37]. In this mechanism, reaction rate is depending on the coverage of pollutant on the catalyst surface. There is a consensus about the effect of initial pollutant concentration on the activity. The idea is that the reaction rate is limited by the Langmuir–Hinshelwood mechanism. In this mechanism, the reaction is zero-order at high concentrations and first-order at low concentrations [18,36,37,39,40,42]. The model of the Langmuir adsorption isotherm is for degradation of NO;

$$r = \frac{dC}{dt} = \frac{kKC}{1 + KC} \quad (2.1)$$

where;

r = rate of reaction

k = limiting rate constant of reaction at maximum coverage under the given experimental conditions

K = equilibrium constant for adsorption of the substrate onto catalyst

C = concentration at any time *t* during degradation

Yu et al. [39], conducted their experiments using different initial NO concentrations ranging from 100 ppb to 1.0 ppm while keeping other conditions as standard. They found higher conversion of NO at lower initial NO concentrations. The rate of the reaction decreases at higher initial NO concentrations.

Hüsken et al. [40], confirmed the results of Yu's study as increasing inlet pollutant concentrations result in lower oxidation rates while lower concentrations enhance performance. They observed that the changes of the NO concentration in the lower range made more remarkable effect on degradation rate of NO than changes in the range of higher inlet concentration.

2.4.4 Total Flow rate

Total flow rate determines the residence time of the pollutants inside the reactor. Residence time refers to time required for the reactants remaining inside the reactor. Low flow rates increases space time while high flow rates decreases it.

Phoocatalytic oxidation time depends on the mass transfer and adsorption of reactants onto the catalyst surface. Flow rate is one of the factors that controls the mass transfer and adsorption of reactant. All the researchers agreed about the effect of the flow rate on the residence time.

Yu et al. [39] investigated varying flow rates for the photocatalytic oxidation of NO. They found that higher conversion is obtained at lower flow rate. Ao and Lee [49] indicated that increasing flow rate from 5 l/min to 30 l/min made NO conversion decrease from 88% to 68%. Hüsken et al. [40] reported the same results that high flow rates decrease the residence time of the NO on the active surface. As a result of that, the degradation rate is reduced.

Similar effects were observed on Devahasdin's study [36] and Wang's study [37]. The conversion increases with increasing of the residence time. But, only difference is that this increase continue until a certain value. After that value, the conversion becomes stable. The system reaches the steady state.

2.4 Kinetic Analysis of Photocatalytic Oxidation of NO_x over TiO_2

Langmuir-Hinshelwood mechanism is widely used to describe reaction mechanism of photocatalytic oxidation of NO [18,36,37,39,40,42]. The holes, $^{\bullet}OH$ radicals, O_2^-, H_2O_2 , and O_2 have important effect on the photocatalytic reaction mechanism with respect to reaction conditions[14].

Devahasdin [36] tried to explain reaction mechanism of photocatalytic oxidation of NO_X over the TiO_2 with UV light. He proposed a reaction mechanism given in Figure 5.

$$\begin{array}{l} NO + \bullet OH \leftrightarrow HNO_2 + \bullet OH \leftrightarrow NO_2 + H_2O \\ \qquad\qquad\quad \uparrow\downarrow \qquad\qquad\quad \uparrow\downarrow +e^- \\ \qquad\qquad H^+ + NO_2^- \leftrightarrow NO_2 \quad NO_2^- \\ \qquad\qquad\quad\ +e^- \end{array} \qquad \text{(a)}$$

$$\begin{array}{l} \qquad\quad hv \\ NO_2 + \bullet OH \leftrightarrow HNO_3 \\ \qquad\quad \uparrow\downarrow \\ \qquad\ H^+ + NO_3^- \end{array} \qquad \text{(b)}$$

Figure 5. Reaction networks for photocatalytic oxidation of NO_x on the surface of the TiO_2 [36]

The summary of the photocatalytic oxidation reaction of NO over TiO_2 is that NO is consumed to produce HNO_2 quickly at initial period. There is no observation of NO_2 in this period. At the transient period, HNO_2 is converted to NO_2. Then, NO_2 is oxidized to HNO_3.

Later, the domination of stable HNO_3 and its dissociated ions take place. The gas phase NO_2 is in equilibrium with the adsorbed NO_2 during the transient period. After transient period, the steady state is reached. At a short space time, NO_2 is the point that the oxidation reaction can only reach. At a long space time, pseudo-equilibrium for all fast reactions are established. When the UV light reaches to the TiO_2 surface, Devahasdin et al. [36] presented the reaction regimes as shown in Figure 6.

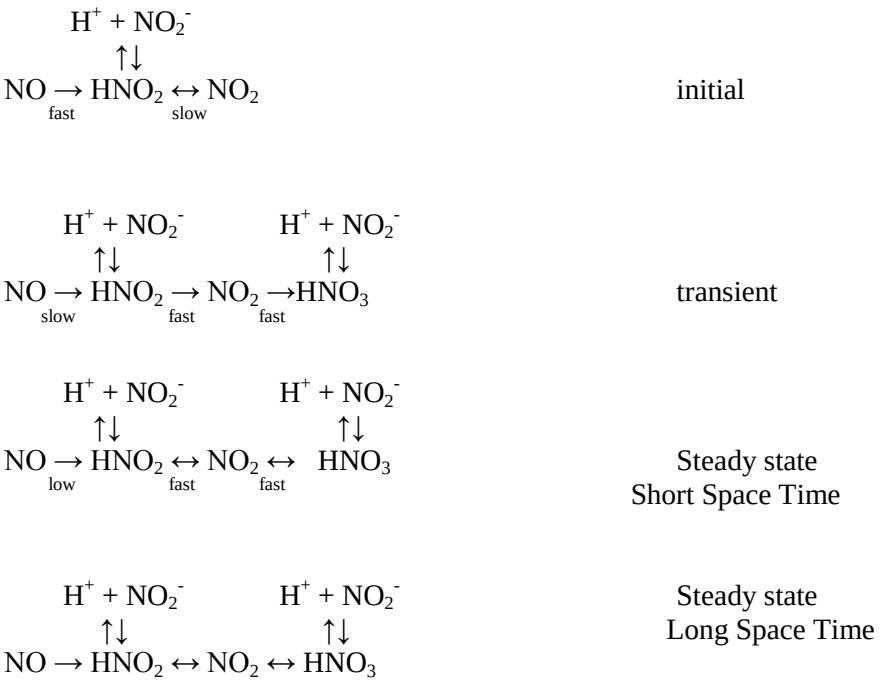

Figure 6. Reaction shemes for photocatalytic oxidation of NO by using TiO_2 as catalyst[36]

Wang et al. [37] proposed a reaction mechanism in the light of their research in Figure 7. They are consistent with the results of Devahasdin et al.[36]. They also proposed an additional reaction process to obtain improved fit of the reaction mechanism to the data. They also showed the role of oxygen molecules in the mechanism.

$$NO + \bullet OH \leftrightarrow HNO_2 + \bullet OH \leftrightarrow NO_2 + H_2O$$
$$\uparrow\downarrow \quad (a)$$
$$H^+ + NO_2^-$$

$$2NO + O_2^- \xrightarrow{+3e^-} 2NO_2 \quad (b)$$

$$NO_2 + \bullet OH \leftrightarrow HNO_3 \leftrightarrow H^+ + NO_3^- \quad (c)$$

$$3NO_2 + 2OH^- \leftrightarrow 2NO_3^- + NO + H_2O \quad (d)$$

Figure 7. Reaction mechanism proposed by Wang et al. [37]

Yu et al. [50] studied kinetics of indoor air purification by heterogeneous photocatalytic oxidation. The kinetic study they made shows good compatibility with their experimental results. In their work, the photocatalytic oxidation of NO starts with adsorption of H_2O, O_2 and NO in the presence of visible light.

$$TiO_2 + H_2O \overset{K_{H_2O}}{\longleftrightarrow} T\dot{i}O_2\_H_2O \quad 1$$

$$TiO_2 + O_2 \overset{K_{O_2}}{\longleftrightarrow} T\dot{i}O_2\_O_2 \quad 2$$

$$TiO_2 + NO \overset{K_{NO}}{\longleftrightarrow} T\dot{i}O_2\_NO \quad 3$$

Generation of electron/hole pairs and trapping of the generated electron/hole pairs are the first step that is shown as follows.

$$TiO_2 + H_2O \xrightarrow{\varphi} e^- + h^+ \quad 4$$

$$h^+ + TiO_2\_H_2O \xrightarrow{k_{h^+}} OH\bullet + H^+ \quad 5$$

$$e^- + TiO_2\_O_2 \xrightarrow{k_{e^-}} O_2^- \quad 6$$

Second step is oxidation of NO by hydroxyl radicals. The final product was obtained as NO_3^-.

$$TiO_2\_NO + OH\bullet \rightarrow TiO_2\_HNO_2 \qquad 7$$

$$TiO_2\_HNO_2 + OH\bullet \rightarrow TiO_2\_NO_2 + H_2O \qquad 8$$

$$TiO_2\_NO_2 + OH\bullet \rightarrow NO_3^- + H^+ \qquad 9$$

In the initial region, the major processes with their characteristic times in Figure 2 determine the kinetics of the oxidation process. The reaction rate model for NO and NO_2 was taken from Yu's study[50]. Reaction rate model was predicted in the light of Langmuir-Hinshelwood model which was developed by using the Langmuir adsorption isotherm. The reaction rate model for NO was derived as Eqn 2.2. Their reactor assumption is the plug flow reactor for the full model of NO and NO_2 concentration in the reactor.

$$r_{NO} = \frac{-k_{NO}C_{TiO_2\_NO}\gamma C_{TiO_2\_H_2O}}{4k_{NO}C_{TiO_2\_NO} + 2k_{NO_2}C_{TiO_2\_NO_2}}\left(\sqrt{1+\frac{4\alpha E}{\gamma C_{TiO_2\_H_2O}}}-1\right) \qquad (2.2)$$

The reaction rate model for NO_2 was derived as Eqn 2.3.

$$r_{NO_2} = \frac{\left(-k_{NO}C_{TiO_2\_NO} - k_{NO_2}C_{TiO_2\_NO_2}\right)\gamma C_{TiO_2\_H_2O}}{4k_{NO}C_{TiO_2\_NO} + 2k_{NO_2}C_{TiO_2\_NO_2}}\left(\sqrt{1+\frac{4\alpha E}{\gamma C_{TiO_2\_H_2O}}}-1\right) \qquad (2.3)$$

respectively, where

$$\gamma = \frac{k_{h^+} \times k_{e^-}^*}{k_{dea}} \qquad (2.4)$$

$$\beta = \frac{k_{h^+} \times k_{e^-}^*}{k_{dea}} \times C_{TiO_2} \qquad (2.5)$$

$C_{TiO_2\_NO}$, $C_{TiO_2\_NO_2}$ and $C_{TiO_2\_H_2O}$ are the adsorbed gas concentrations and given by Eqn. 2.6, 2.7 and 2.8.

$$C_{TiO_2\_NO} = \frac{K_{NO} C_{TiO_2} C_{NO}}{1 + K_{NO} C_{NO} + K_{NO_2} C_{NO_2} + K_{H_2O} C_{H_2O}} \quad (2.6)$$

$$C_{TiO_2\_NO_2} = \frac{K_{NO_2} C_{TiO_2} C_{NO_2}}{1 + K_{NO} C_{NO} + K_{NO_2} C_{NO_2} + K_{H_2O} C_{H_2O}} \quad (2.7)$$

$$C_{TiO_2\_H_2O} = \frac{K_{H_2O} C_{TiO_2} C_{H_2O}}{1 + K_{NO} C_{NO} + K_{NO_2} C_{NO_2} + K_{H_2O} C_{H_2O}} \quad (2.8)$$

where;

C is concentration (mol/l)

E is irradiance on the surface of photocatalyst (W/m^2)

k is reaction rate constant (dm^2/mol.min)

K is adsorption constant (l/mol)

α is the parameter, irradiance related (mol W^{-1} min^{-1})

γ is a group of parameters of k_{h^+}, $k^*_{e^-}$ and k_{dea} (min^{-1})

β is a group parameters of γ and sites

2.5 Preparation of TiO_2 As a Thin Film

Kemmit et al. [51] indicated that traditional thin-film coating methods are mostly not appropriate to coating because of the high calcination temperature between 400 and 600°C. This temperature make difficult to develop the photoactive anatase phase.

There are many techniques to prepare thin film coating for TiO_2 such as sol-gel method, vapor phase process, evaporation, chemical vapor deposition, ion beam techniques and reactive D.C. or dioxide or magnetron sputtering. Sol-gel method is mostly used technique for coating in the literature. Zhu et al. [52] reported that the sol-gel processing is very attractive due to being versatile synthesis procedures and allow the formation of nanostructured materials with controlled shape and porosity. Brinker and Harrington [53] determined that the sol-gel processing is an effective method to produce transparent, thin, multi-component oxide layers of many compositions on various substrates.

Sol–gel processes depend on the polycondensation and hydrolysis of various titanium molecular precursors in an organic solvent or aqueous solution. Sol-gel process is used with

spin or dip coating techniques. The sol-gel process has a precursor (metal alkoxides), catalyst (acetic acid), solvent (alcohol) and gelation (water). After getting solution, spin or dip coating can be applied.

Ganesh et al. [54] mentioned that these techniques face certain limitations. Sol–gel is a volatile technique and it is difficult to control the thickness of the deposited film. Sputtering is basically a batch process. It is time consuming and costly. CVD is a continuous processing method. In this method, precursor compounds in the gas phase react and precipitate on the surface of the glass. Though the process parameters can be accurately controlled by this technique, it is still an expensive method. He reported that use of electro spinning to produce a transparent, photocatalytic, and super hydrophilic TiO_2 coating on glass substrates after getting sol-gel solution.

Celik et al. [55] also prepared self-cleaning Al_2O_3–TiO_2 thin films on glass substrate for photocatalytic applications. They used a sol-gel technique. They used scratch tester, UV/Vis spectrometer, SEM and XRD to show the adhesion and optical properties, phase structure, microstructure of the coatings. They obtained that the oxide films were active for photocatalytic decomposition of methylene blue.

2.6 Water De-Nitrification

High levels of nitrogen to rivers, primarily in the form of nitrate (NO_3^-), can threaten ecosystem and human health such as causing algal and dinoflagellate blooms, fish kills, eutrophication, hypoxia, groundwater contamination, blue baby syndrome and cancer, especially of the stomach. Major sources of nitrogen in the rivers are the diffusion of excess nitrogen added to soils, runoff and leaching in non-cultivated areas and urban or industrial wastewater treatment plants [56,57]. Reverse osmosis and electrodialysis, advanced filtration and biological denitrification, ion exchange are the some available treatments for the removal of nitrogen from aqueous media. The phsico-chemical methods have high processing costs. Biodenitrification has long contact time, incomplete denitrification and the residual organics from the organic compounds supplied as energy source. In the presence of noble- or transient metal catalyst, ammonium formation is still a severe problem [58]. So, photocatalytic denitrification is an alternative way due to having environmental benefits compared to other treatments and economically viable process [57].

Anderson J. A. [59] underlined that while the volume of accessible data for organic reagent destruction is huge, the amount of studies related to photocatalytic nitrate removal is limited.

Luiz et al. [57] determined that TiO_2 based photocatalytic catalysts with formic acid as a hole scavenger can have high selectivity toward N_2, high conversion of nitrate and high photocatalytic activity. Zn-TiO_2 has a great potential due to selectivity in the conversion to

N_2 (95.5 %), nitrate conversion (92.7%) and photocatalytic activity (14.2 $\mu mol_{NO3} - (min\ g_{catalyst})^{-1}$). Formic acid can be completely converted into CO_2 and H_2O compounds.

CHAPTER 3

MATERIALS AND METHODS

In this chapter, materials and methods used to determine the NO oxidation ability of TiO_2, pure, in-the grout and in the plaster samples will be given. Firstly, materials and their preparation methods are described. Then the experimental set-up based on ISO-22197:2007(E) standard is explained. Finally, the measurement methodology is presented.

3.1 Materials

Three samples of titanium dioxide were used. One of them was Degussa (Evonik) P25, AeroxideTiO2 P25, supplied by Evonik Industries. The second one was obtained by Titanium(IV) isopropoxide (purity 97%) from Sigma-Aldrich Chemie GmbH. TiO_2 in the grout and in the plaster samples were prepared by Kalekim Company. Other commercial chemicals were acetic acid with 99-100 % purity (J. T. Baker Company), ethanol with 99.7% purity (J. T. Baker Company).

3.2 Sample Preparation

Two different sample categories were investigated. The first group of samples was TiO_2 mixed in with a cement based material such as grout or plaster. The second type of sample was coated on grout, plaster or glass. Two different coating methodologies were also used as sol-gel coating and doctor blade coating. The coating on a glass substrate was done by sol gel and doctor blade methods. The coating on the grout samples were only done by doctor blade method. Grout preparation was presented in detail in Oymak's PhD Thesis [60].

3.2.1 Coating Methodology

In the doctor blade method, firstly, pure TiO_2 (Degussa (Evonik) P25) powder is mixed with deionized water in a bowl. Then aqueous TiO_2 slurry is put on the glass by the help of a pipette and coated as a thin film over glass or grout surface by a flat blade. The desired amount of TiO_2 on the surface was adjusted by pipette. To obtain different thickness on the film, amount of TiO_2 put on the glass and grout was changed. Finally, the samples were cured at room temperature for 24 hours.

In the sol-gel method, it is desired to produce a transparent, photocatalytic, and superhydrophilic TiO_2 coating on glass substrates after getting sol-gel. Titanium(IV) isopropoxide (TIP) is commonly used as a precursor for the preparation of TiO_2. Firstly, the glass surface is roughened by HCl in the ultrasonic bath to hold TiO_2 particles on the surface easily. Then, 6.3 ml of TIP with 98% purity, 5 ml of acetic acid with 99.5% purity and 50 ml of ethanol with 99.7% purity is mixed for preparing sol-gel solution. The change on the TIP amount determines the TiO_2 amount in the mixture. The mixing procedure is that 5 ml of acetic acid is added to ethanol inside the bowl and stir for 5 min. Then, add the TIP and mix for 2 minutes and wait for 24 hours. Finally, the gel is obtained. Dip-coating is applied to the glass. The glass is dipped in the gel at 20 mm/sec rate. It is removed from the gel at 2 mm/sec rate. Then, the sample was calcinated at 400^0C for 2 hours.

3.2.2 In The Grout Preparation (Commercial Samples)

Ten different grout samples prepared by Kalekim with different TiO_2 amounts were tested. Hombikat N100 with 20 nm particle size, 100 m^2/g surface area and containing 98% TiO_2 (anatase) was used in these samples. The samples were divided to two different types, namely plaster and grout. The sample type and the percentage of TiO_2 determine the name of the test piece. For example, S2 is the name of the test piece. 2 refers that test piece has 2% TiO_2 and S indicate plaster while grout is shown as D. The detailed information about commercial samples was given in Oymak's PhD Thesis [60].

3.3 Experimental Set-Up

NO oxidation is a diagnostic tool for photocatalytic activity. The only standard method validated to analyze photocatalytic activity of oxidation of NO_X is ISO-22197:2007(E) standard. The scope of the test set-up is to determine the air-purification performance of materials having photocatalytic films on the surface or a photocatalyst, usually contains semiconducting metal oxides, like titanium dioxide or other ceramic materials, by continuous exposure of a specimen to the model air pollutant under illumination with UV light. It is not

suitable for the determination of other performance attributes of photocatalytic materials, i.e., decomposition of water contaminants, self-cleaning, antifogging and antibacterial actions. The experimental set-up is shown in Figure 8. 3D view and top view were also drawn in Figure 9 and 10, respectively.

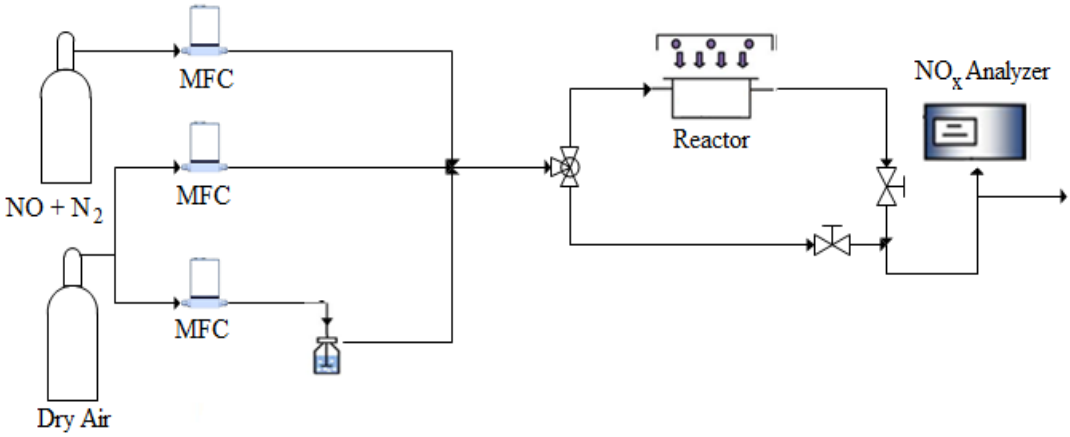

Figure 8. A schematic of the test equipment

There are four main parts in the set-up:

- A test gas supply
- A photoreactor
- A light source
- NO_x analyzer

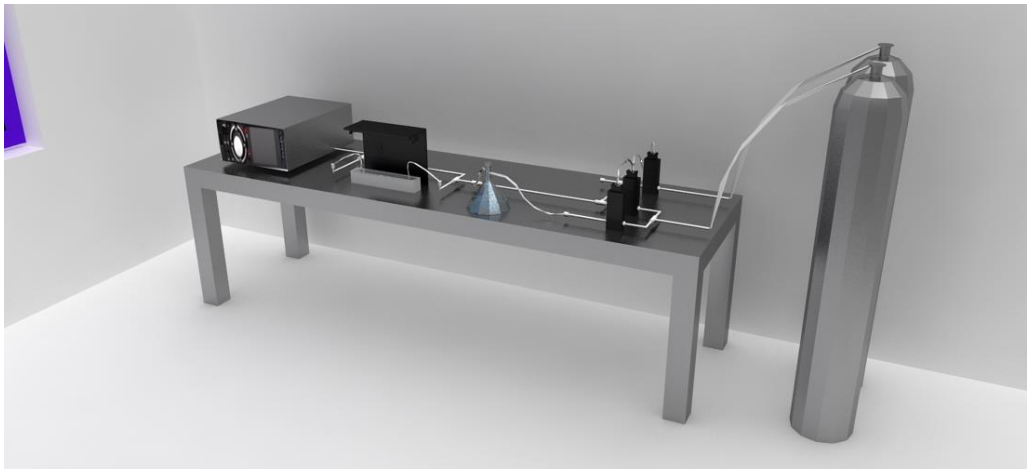

Figure 9. 3-D view of the test equipment

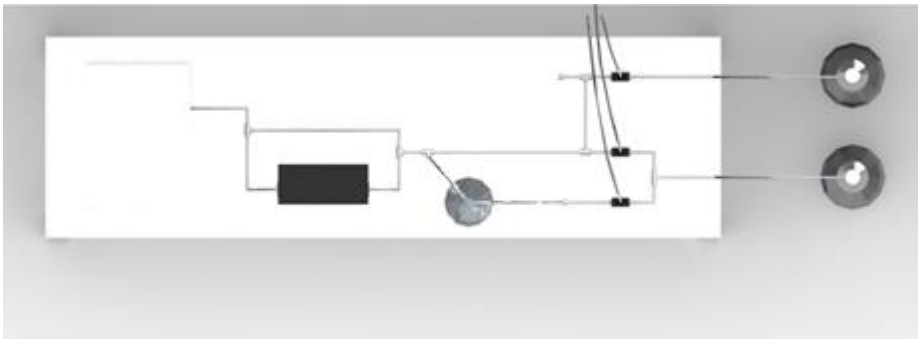

Figure 10. 3-D top view of the test equipment

The system was constructed with stainless steel, because low concentrations of pollutants are to be tested. Stainless steel is a material of low adsorption and resistant to ultraviolet (UV) radiation.

A test gas supply is the entrance unit to the system. This unit consists of two parts; three mass flow controllers and one humidifier. One of the mass flow controllers has maximum 100 ml/min flow of pollutant gas which contains NO gas while each of the other two flow

controllers has maximum 2000 ml/min flow of air. Humidifier is used as adjusting relative humidity in the system.

The photoreactor is made up of a stainless steel body and a quartz optical window. The dimensions of the stainless steel are 36 cm length, 6 cm width and 6 cm height. There is a sample location with 10 cm length, 5 cm width and 5 mm height inside the reactor. In addition, there is 5 mm thick air layer between optical window and sample surface. The schematic view of the photoreactor is seen in Figure 11.

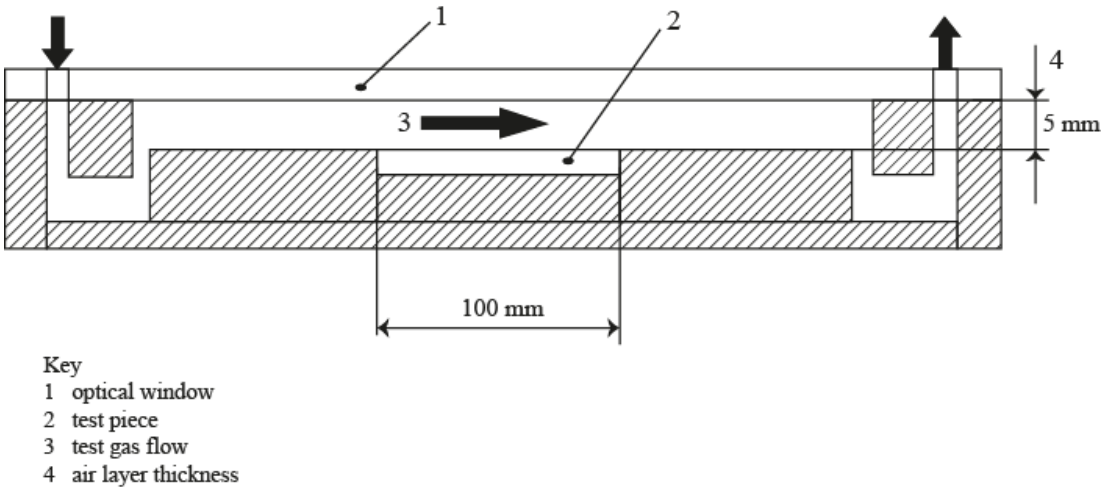

Figure 11. A cross-sectional view of the photoreactor

Blacklight blue fluorescent lamp with 15 watts is used as the light source. The wavelength of the lamp is 365 nm and provides UV-A illumination. The light irradiates uniformly the test piece.

NO_x analyzer is the Model 42i Chemiluminescence NO-NO_2-NO_X Analyzer from Thermo Fisher Scientific Inc. to use determines the NO, NO_2 and NO_x concentration in the system. The principle of operation of the analyzer is explained in the next section.

3.3.1 Principle of Operation of Chemiluminescence NO-NO_2-NO_x analyzer

Chemiluminescence NO-NO_2-NO_x analyzer which is the Model 42i is used for determining NO, NO_2 and NO_x concentration. The principle of the analyzer is that nitric oxide (NO) reacts with ozone (O_3) to produce a characteristic luminescence with intensity linearly proportional to the NO concentration. In other words NO_2 in an excited state is formed as a result of this reaction.

The chemiluminescent detector has basically the following reactions;

$$NO + O_3 \xrightarrow{k_1} NO_2^* + O_2 \qquad 10$$

$$NO_2^* \xrightarrow{k_2} NO_2 + hv \qquad 11$$

$$NO_2^* + M \xrightarrow{k_3} NO_2 + M \qquad 12$$

The first reaction 10 is the reaction between NO and O_3 to form excited nitrogen oxide (NO_2^*). Then, there is equilibrium through chemiluminescence (reaction 11) or collisional energy transfer with any third body (reaction 12).

The schematic view of chemiluminescence analyzer is shown in Figure 12. There are two inlets to the analyzer. One of them is dry air which passes through a flow switch, and then through a silent discharge ozonator to generate ozone. Ozone is needed for chemiluminescent reaction. The ambient air sample is drawn into the analyzer from the other inlet. The sample flows through a capillary and then to the reaction chambers as NO mode and NO_x mode by the help of the mode solenoid valve. While NO mode is used to calculate the NO concentration in the sample, NO_x mode determines the NO_x concentration in the sample. In the NO_x mode, there is a molybdenum NO_2-to-NO converter heated to about 325^oC that converts NO_2 in the sample to the NO. Reaction 4 takes place in the molybdenum NO_2-to-NO converter. Therefore, the NO concentration with the converted NO is the NO_x concentration in the sample flow.

$$3NO_2 + Mo \rightarrow 3NO + MoO_3 \qquad 13$$

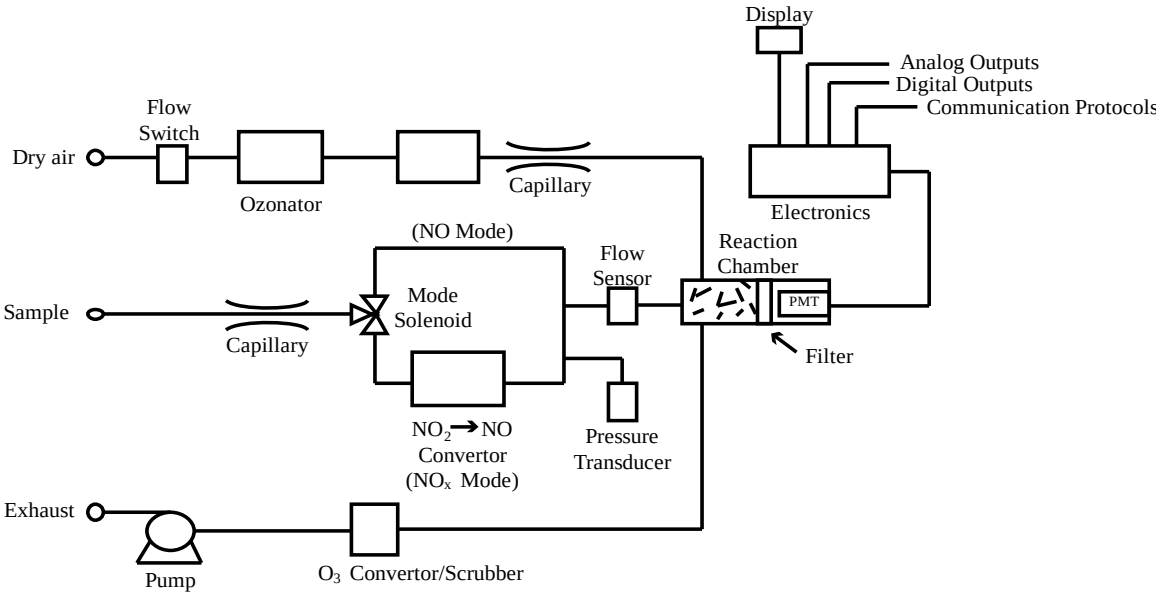

Figure 12. The Model 42i flow schematic

A photomultiplier tube (PMT) detects the luminescence generated during the reaction. In this analyzer, the NO and NO_x concentrations are calculated and the difference between them shows the NO_2 concentration. The NO_2 concentration is not directly calculated from the analyzer. Calibration of NO_x analyzer is described in Appendix A.

3.4 Experimental Procedures

3.4.1 Experiments in the Light of ISO Standard

In the light of ISO-22197:2007(E) standard, experiments were generally conducted as follows:

Pretreatment of the test piece was explained in ISO standard as two parts: removing of organic compound and washing with water. Test pieces were only washed with water. The detailed information for pretreatment of test pieces is in Appendix D.

Thereafter, the test piece was placed in the photoreactor. The glass window was attached after adjusting the space between the test piece and the window. At the same time, the flow

was stabilized. An empty line was directly connected to the NO_x analyzer. This stabilization was made by using this empty line.

Then, the test gas was allowed to flow into the photoreactor, without photoirradiation. The flow rate of the dry air and pollutant gas (contains 100 ppm NO and balance N_2) was adjusted according to desired value. The measurement of relative humidity was made before the experiment by using a Testo 410-2 device for humid air property measurements. The relative humidity measurement point was entrance of the reactor. Irradiance from the light source was measured in Physics Department in METU. The experimental set-up was simulated during the light intensity measurements. The test gas was allowed to flow for 30 min. In this period, the change in the volume fraction of NO and nitrogen dioxide (NO_2) were recorded under dark conditions. If the NO*x* volume fraction was less than 90 % of the inlet volume fraction after 30 min, it should be waited until it exceeded that value.

After dark condition, the gas flow was maintained and irradiation of the sample was commenced, and the NO and NO_2 volume fractions under photoirradiation was recorded for minimum 1 hour, because the system in this study reached steady state at minimum 1 hour. Next, photoirradiation was stopped. The zero-calibration gas was switched to under the same flow conditions. At the same time, the NO*x* volume fraction was recorded for 30 min. Finally, the gas supply to the reactor was stopped and the test piece was removed from the reactor.

3.4.2 Measurement of the Start-Up Effect

This experiment was performed with an empty photoreactor. At the same time, the flow was stabilized entering empty line directly connected to the NO_x analyzer by valve. Then, the test gas was allowed to flow into the photoreactor, without photoirradiation. The flow rate of the dry air and pollutant gas (contains 100 ppm NO and balance N_2) was adjusted according to desired value. The flow was continued for 30 min and the change in the volume fraction of NO and nitrogen dioxide (NO_2) was recorded under dark conditions. Finally the gas supply to the reactor was stopped.

3.5 Measurement of Heats of Hydration and Oxygen Adsorption by Microcalorimetry

In this measurement, a previously constructed home built system was used. This system contains a Setaram C-80 Tian-Calvet Calorimeter, Pfeifer turbo molecular pump station, a Baratron gauge (Varian CeramiCel) and a multi-port high-vacuum Pyrex glass manifold. The details of the home made systems are given in Uner et al.'s study [61]. The schematics of the adsorption manifold are given in Figure 13.

In the set-up, there are four valves. First valve is used to control the vacuum pump. The second one is opened to the barometer. The third one is connected to the microcalorimetry. The fourth one is used to supply saturated air to the main part of the system. The temperature of the main part is kept at 50 ^{o}C. At first, three valves except fourth one are closed. 0.5 gram TiO_2 is placed to the microcalorimeter. The temperature is kept at 100 ^{o}C. The first valve is opened. All air in the main part is taken. Then, the third valve is opened. The system is kept in the vacuum for a day. As a result, most of the water adsorbed on the surface of the sample is removed. The water vapor saturated at 25 ^{0}C is obtained in the closed part. Then, the first and third valves are closed. The fourth valve is used to supply the water vapor to the apparatus. Afterwards, the fourth valve is also closed. The first valve is used to obtain the desired pressure in the main part. After pressure adjustment, the first valve is closed. The third valve is turned on. After this process, specimen heat flow can be precisely recorded continuously. The same procedure was applied to determine oxygen adsorption over 0.5 gram TiO_2 using oxygen rich gas (balance N_2) instead of saturated air.

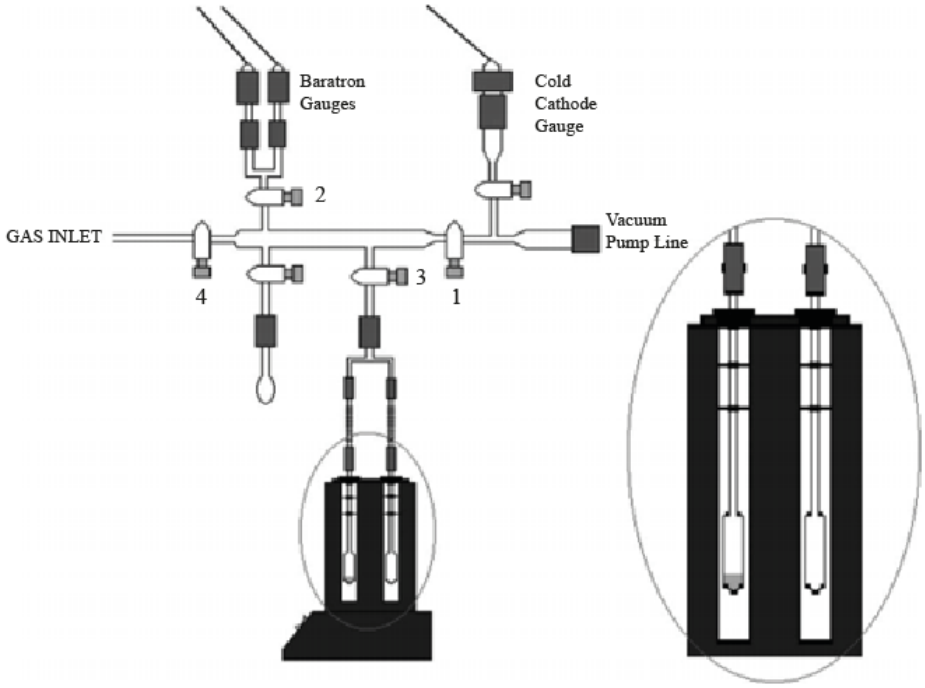

Figure 13. The schematic drawing of the set-up and the sample-reference cell configuration for the microcalorimetry [61].

CHAPTER 4

RESULTS AND DISCUSSION

The objective of this study is to construct a NO_X analysis test system based on ISO-22197:2007(E) standard that can monitor NO oxidation ability of photocatalytically active surfaces. The fundamental experiments were conducted in the light of ISO standard. Firstly, the photocatalytic activity of the pure TiO_2 on the surface of the glass and the grout was observed. Then, sol-gel method and doctor blade method were tested in the set-up. Activities of commercial samples were also discussed in Chapter 4. Improvements and modifications for ISO standard are recommended by start-up experiments. In addition, a fundamental study about the effects of different parameters on photocatalytic oxidation of NO_x such as relative humidity, catalyst loading, total flow rate and inlet concentration was presented. Water and oxygen adsorption on TiO_2 is analyzed by Microcalorimetry. Finally, some comments were made in the light of the experimental data in this study.

4.1 Glass and Grout Coating

Coating was applied on the grout and glass. The surface coated samples were tested for NO oxidation activity and the results are presented in Figure 14. The similarity of the data indicates that the coating on the grout and on the glass show similar performance even though the samples are obtained from different sources and are coated on different substrates.

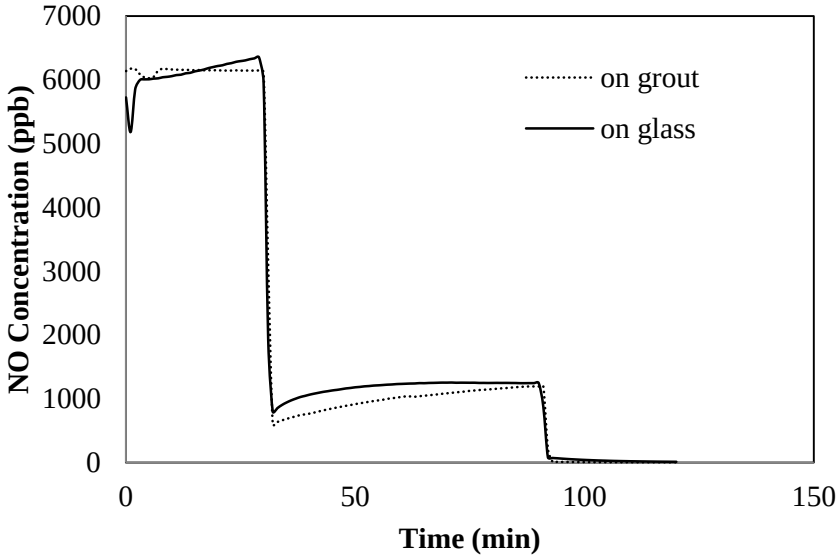

Figure 14. NO oxidation activity of surface coated TiO_2 on the grout and on the glass: inlet total flow rate is 1l/min, light intensity is 18.8 W/m^2, relative humidity is 50%

4.2 Sol-Gel Method

Coating method has a vital role on photocatalytic oxidation of NO. Doctor blade method and sol-gel method were used. The coated samples were pictured in Figure 15. The difference on the coating methods was shown in Figure 16. The activity is higher on doctor blade method due to loading higher catalyst amount. But, the sol gel method makes the glass more transparent. XRD analysis indicated that anatase phase was dominant on all of the samples as seen in Figure 17.

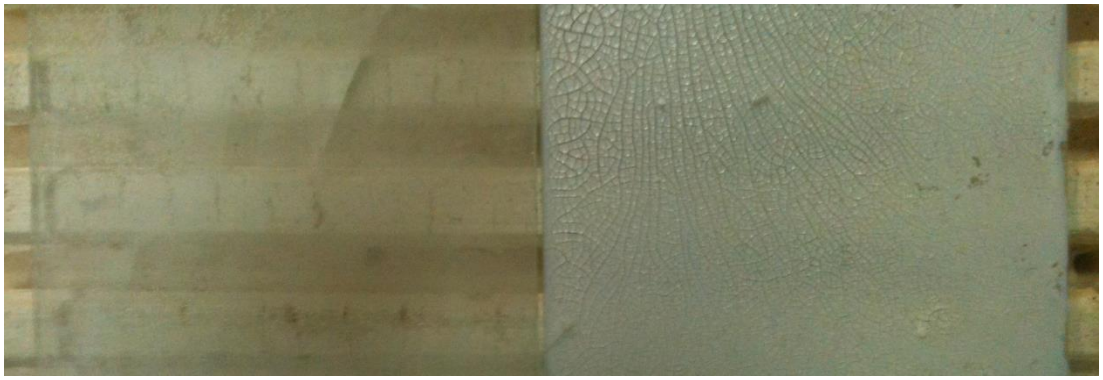

Figure 15. Picture of glasses coated by sol-gel method (on the left side) and doctor blade method (on the right side)

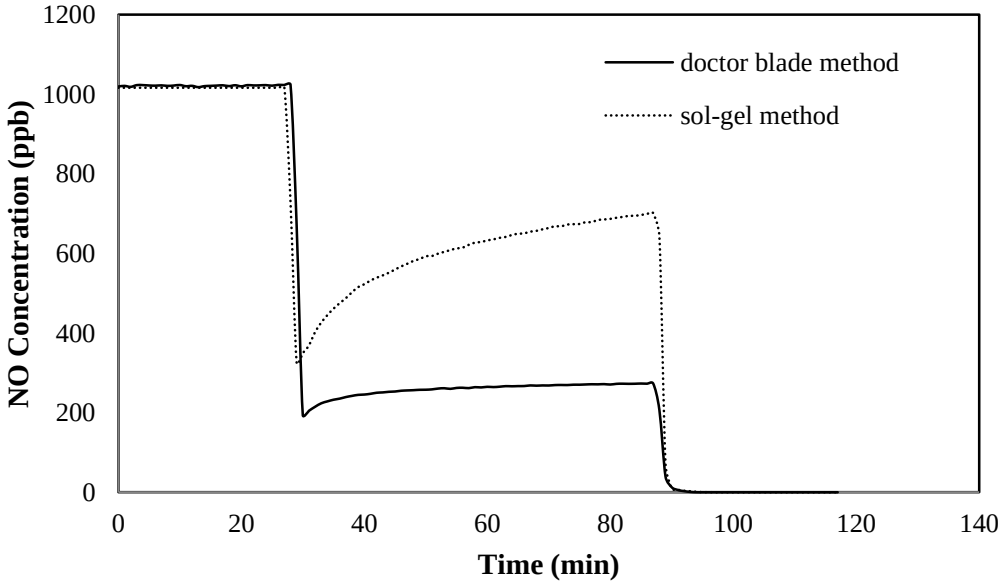

Figure 16. Comparison of doctor blade method and sol-gel method at the same reaction conditions: total flow rate is 1 l/min, relative humidity is 50%, light intensity is 18.8 W/m^2, inlet NO concentration approximately is 1 ppm.

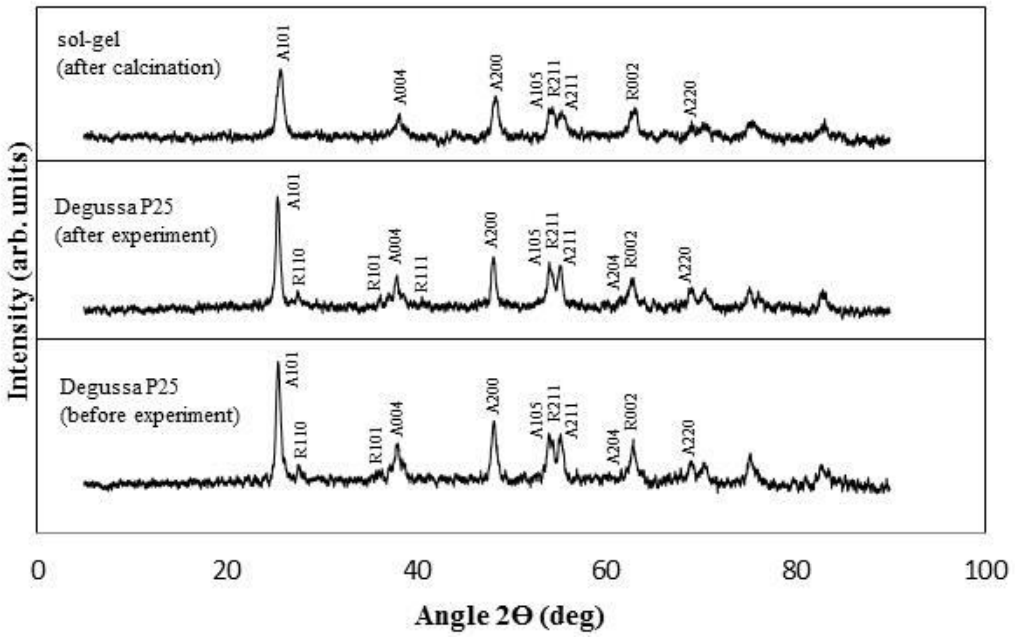

Figure 17. XRD characterization of TiO_2 prepared by sol-gel and two different Degussa P25 samples

4.3 In The Grout Preparation

The samples from Kalekim A.Ş. are tested and results are shown in Figure 18 and 19. S and D samples are used. S refers to grout (sıva) and D refers to plaster (derz) sample types which are manufactured by Kalekim A.Ş. Increasing catalyst loading results in increasing activity of specimens. The highest activity is observed on S10 in Figure 18 and D10 in Figure 19. S type sample has more catalytic activity on higher catalyst amount. The reason of higher activity is that there may be more adsorption sites on the surface of S type sample. At the certain amounts, there is a similarity on the activity. S4 and S7 samples show very similar activity while D4 and D7 samples have the same impact.

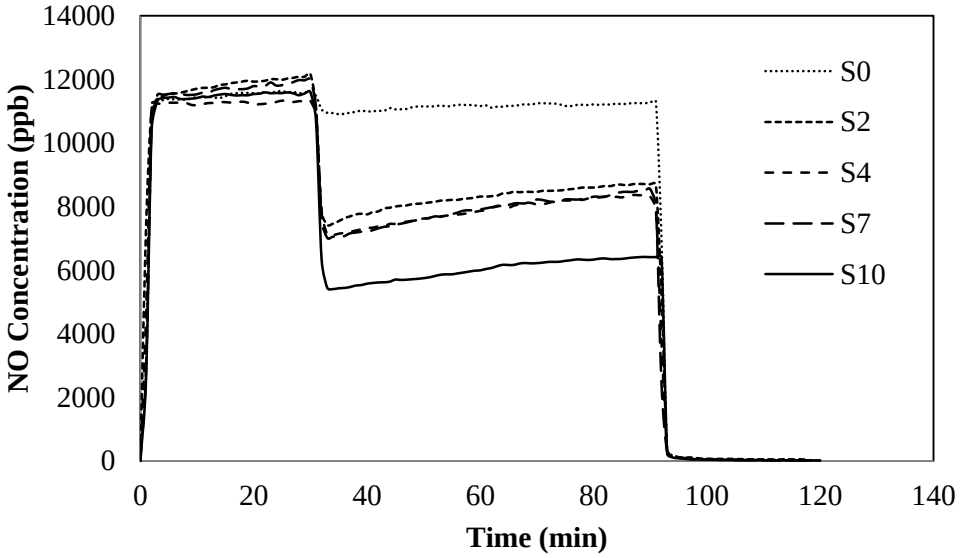

Figure 18. The effectiveness of in-the-plaster (S) samples with respect to time: total flow rate is 1 l/min, relative humidity is 50%, light intensity is 18.8 W/m^2, inlet NO concentration approximately is 12 ppm.

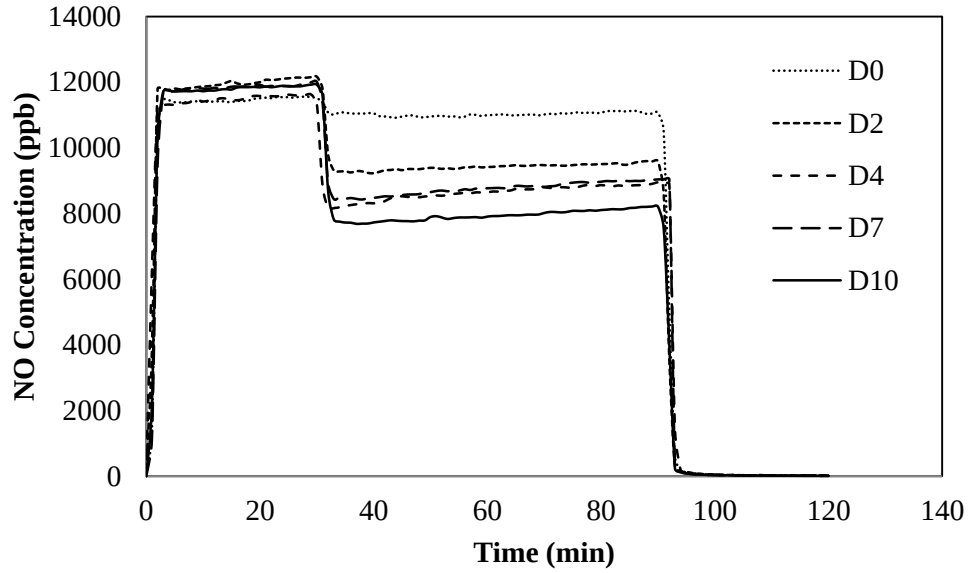

Figure 19. The effectiveness of in-the-grout (D) samples with respect to time: total flow rate is 1 l/min, relative humidity is 50%, light intensity is 18.8 W/m^2, inlet NO concentration approximately is 12 ppm.

According to Figure 18 and 19, amount of NO removed by test piece, amount of NO_2 formed by test piece were calculated when light was on and amount of NOx desorbed by test piece was also calculated when light was off. The quantitative results of the data presented in Figure 19 for D samples and S samples are given in Table 10 and in Table 11, respectively.

4.4 Effect of the Startup On the Inlet Concentration

The empty channel experiments were performed to measure the recovery time of the empty reactor to the steady state concentration. In this study, the used ISO standard for the system to determine photocatalytic activity of cement based materials which contain TiO_2 has missing information in the adsorption part after the first contact time. In the standard, the amount of NO_x adsorption by the test piece is calculated by using data at the time between contact start and when the light is switched on. But in this period, the reactor takes time to get uniform concentration distribution of NO_x inside it. Before the reactor, there is a three way valve. One way goes to NO_x analyzer directly and the other way connects the photoreactor to the flow controllers.

Table 10. The results for D samples

Type	% TiO_2	amount of NO removed by test piece (μmole)	amount of NO_2 formed by test piece (μmole)	amount of NOx desorbed by test piece (μmole)
D	0	1270	98.72	579
	2	7240	1780	539
	4	7290	2190	512
	7	8590	2870	510
	10	10470	2570	471

Table 11. The results for S samples

Type	% TiO_2	amount of NO removed by test piece (μmole)	amount of NO_2 formed by test piece (μmole)	amount of NOx desorbed by test piece (μmole)
S	0	1140	213	595
	2	9800	1780	491
	4	9190	2070	491
	7	1090	2050	512
	10	14790	2200	388

When the test piece is replaced in the chamber, evidently, the chamber is filled with air. When the NO_x flow is redirected to the reactor, a sharp decrease occurs in the reactor, simply because of the dilution effect. This was indicated as NO_x absorption in the standard. This sharp decrease also occurs in empty reactor, eliminating absorption on the specimen as a reason for this sharp decrease in NO_x concentration. In Figure 20, the effect of the three different inlet concentrations as 2500 ppb, 5000 ppb and 7500 pbb in the same flow rate 1000 ml/min, on the concentration inside the reactor was demonstrated. While the inlet concentration increases, the decrease of the inlet concentration is higher. The effect of the inlet flow rate at the same concentration is also analyzed in Figure 21. This figure shows that the change on inlet concentration decreases as the flow rate increases. Both of these are straightforward evidences that the sharp initial decrease is not due to the absorption on the specimen but due to the dilution in the reactor until the reactor is filled with pure NO_x. The data is useful as a RTD curve, but should not be interpreted as the adsorption data.

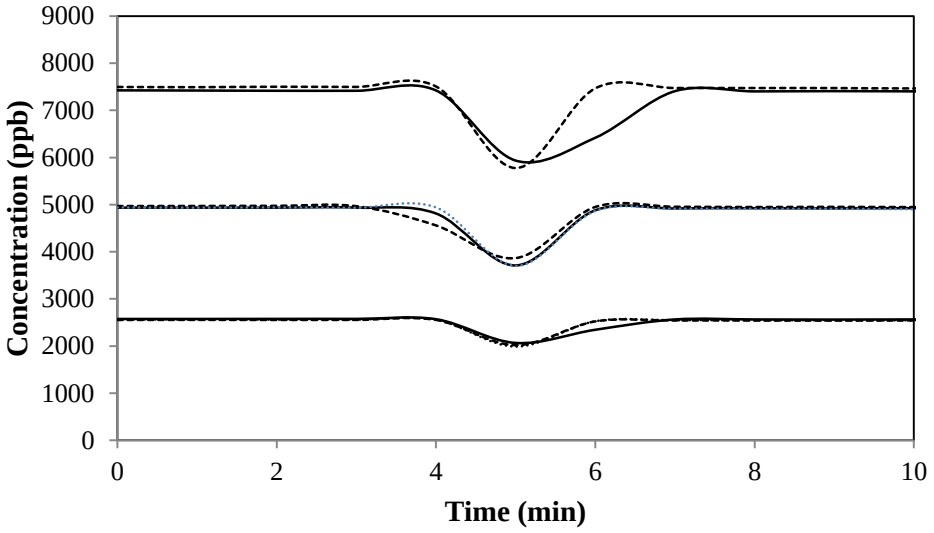

Figure 20. Effect of different inlet concentrations at 1000 ml/min in an empty reactor.

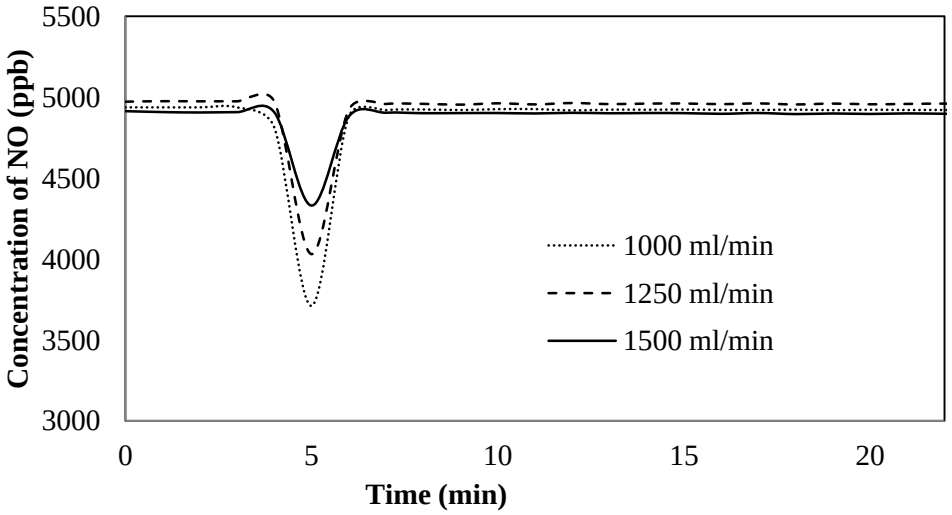

Figure 21. Effect of different flow rates at 5000 ppb inlet concentration in an empty reactor.

4.5 Effects of Different Parameters on Reaction

4.5.1 Effect of Relative Humidity

Relative humidity plays a vital role in these experiments. The reason of that can be seen in the reaction mechanism. In the literature part, different conclusions were made by researchers. The effect of the relative humidity is shown in Figure 22, 23 and 24 for this study. TiO_2 is covered on the glass. The water vapor in air gives hydroxyl groups for oxidation. When relative humidity is zero, the water content inside the catalyst and oxygen molecules in the air is the determining parameter for oxidation. While the water content increase, the photocatalytic activity of the catalyst is improved.

In Figure 22, the effect of the relative humidity (RH) on the NO photo oxidation was demonstrated for the sample with 0.36 g TiO_2, that inlet total flow rate is 1l/min, light intensity is 18.8 W/m^2, inlet NO concentration is 5 ppm. 50% relative humidity was sufficient to trigger the reactions for the samples used in this study. Further experiments were conducted using this value. In Figure 23, NO_2 concentrations in these experiments are presented. Total NO_x concentration analyzed by NO_x analyzer is shown in Figure 24. It is seen that all NO_2 oxidized from NO does not leave the surface. Our experimental results are coherent with Yu's reaction regime [39]. Yu et al. [39] showed that the conversion increases by increasing relative humidity varying from 10% to 70%.

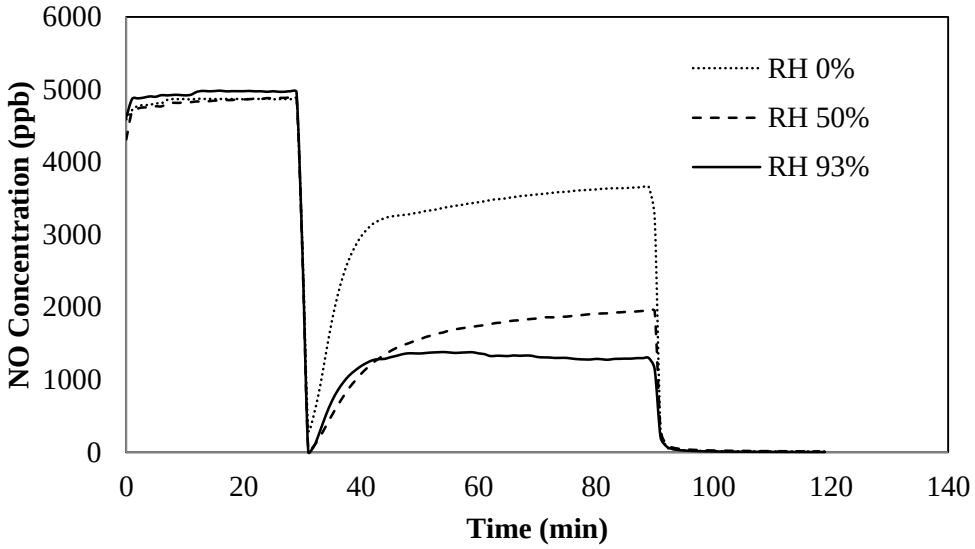

Figure 22. Effect of relative humidity on NO concentration: 0.36 g TiO_2, inlet total flow rate is 1l/min, light intensity is 18.8 W/m^2, inlet NO concentration 5 ppm.

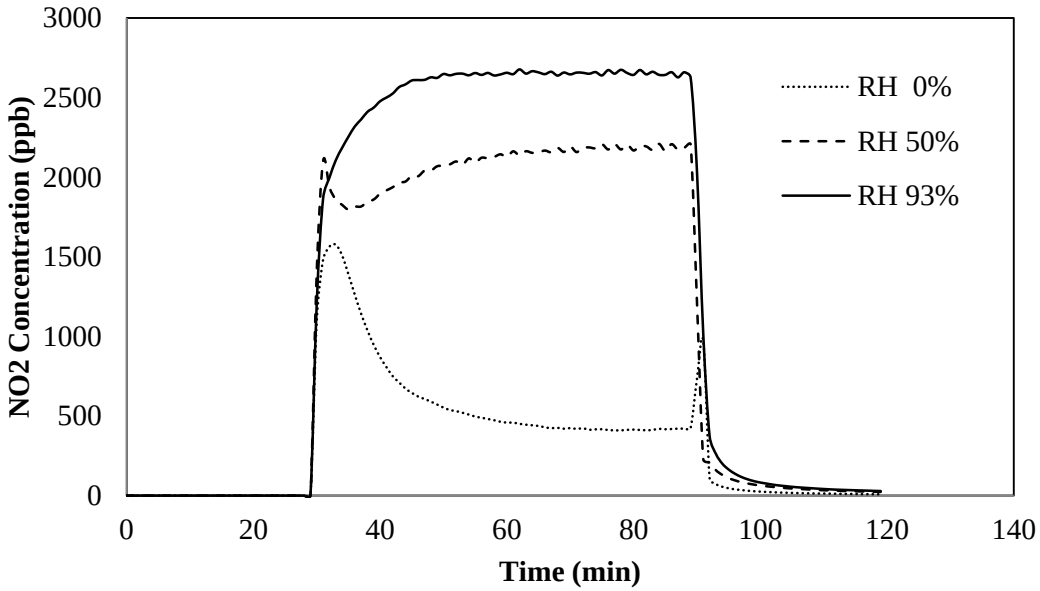

Figure 23. Effect of relative humidity on NO_2 concentration: 0.36 g TiO_2 inlet total flow rate is 1l/min, light intensity is 18.8 W/m^2, inlet NO concentration 5 ppm.

When the RH value is zero, a sharp increase and decrease were observed in the NO_2 concentration. Sharp increase was due to surface-bound hydroxyl radicals formed during washing in the sample preparation. After OH groups were depleted, the rate fell off. The oxygen molecules in the air oxidized the NO in the absence of water molecules in air at 0% relative humidity.

For the 50% relative humidity, the produced NO_2 which was transported form the surface to the air reached the maximum value. Then, adsorption amount of NO_2 increased by consumption of adsorbed NO_2 as a reactant to form NO_3^-. After a certain time, the process reached steady state. When RH was 93%, the initial decrease in NO_2 concentration was no longer observed. The sharp increase at the end of the reaction period for RH 0% sample is due to desorption of the adsorbed species from the surface.

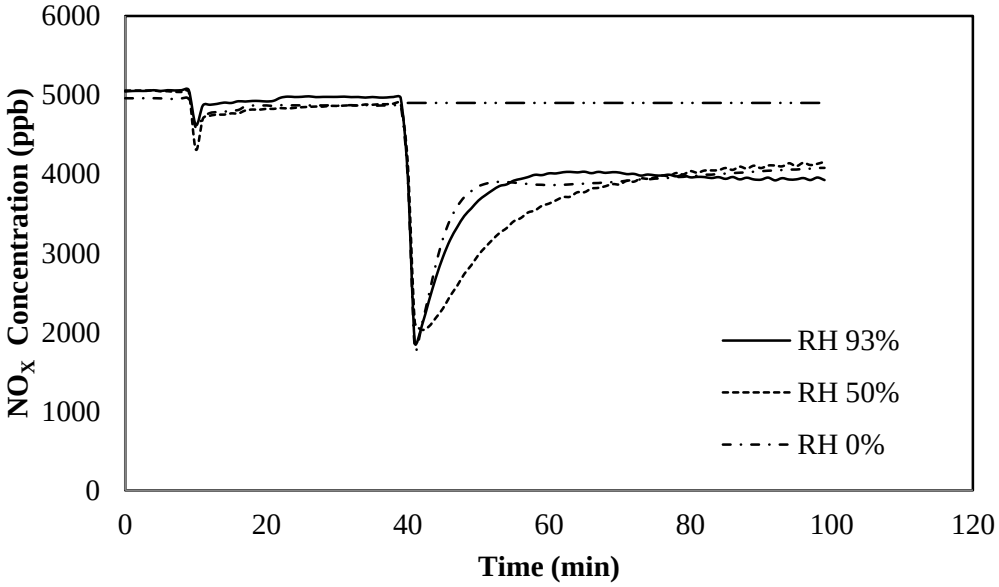

Figure 24. NO_x concentration on different relative humidities: 0.36 g TiO_2 inlet total flow rate is 1l/min, light intensity is 18.8 W/m^2, inlet NO concentration 5 ppm.

In Figure 24, the adsorbed or converted NO_x amounts were shown along with the inlet NO_x concentration curve. The difference between the inlet concentration and measured value constitutes the NO_x remaining on or in the sample. The accumulation NO_X may decrease active sites on the catalyst surface. At steady state after 100 min, the total NO_x amount measured by the analyzer was not affected by the relative humidity which indicates that adsorption of hydroxyl radicals and NO_x may not happen on the same active sites.

In Figure 25, the effect of relative humidity can be observed from 0% relative humidity to 50% relative humidity for two glass coatings. The catalyst loading to each glass was same as 0.36 g. It is seen that 50% relative humidity shows more catalytic activity.

Increasing relative humidity from 50% relative humidity to 75% relative humidity enhances photocatalytic oxidation in Figure 26. Catalyst loading in this experiment was 0.63 g.

Photocatalytic activity of the glass with 0.36 g catalysts loading at 50% relative humidity shows similarity by photocatalytic activity of the glass with 0.63 g catalysts loading at 75% relative humidity.

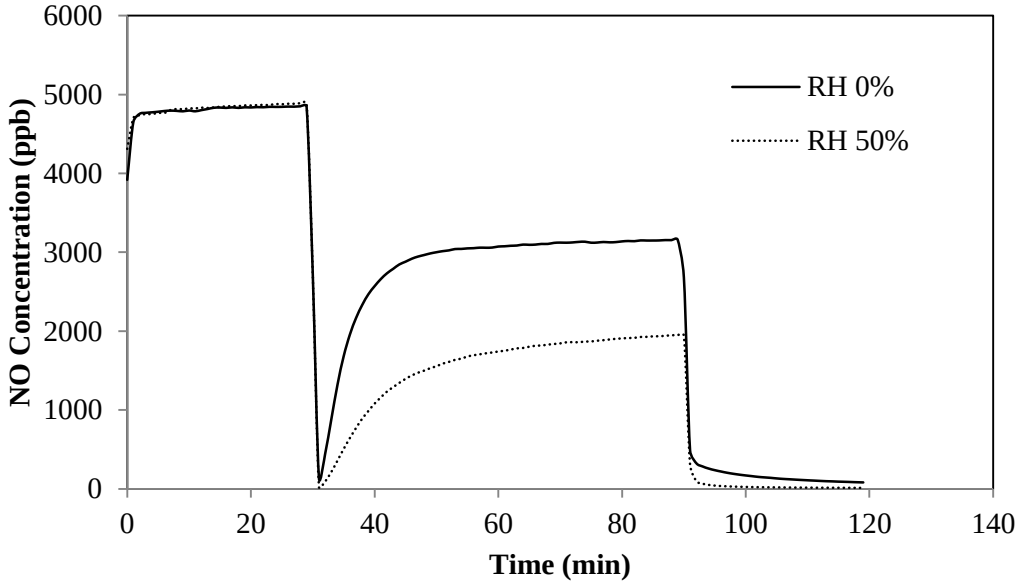

Figure 25. Effect of relative humidity for different samples but same amount: TiO_2 loading is 0.36 g, inlet total flow rate is 1l/min, light intensity is 18.8 W/m^2, inlet NO concentration 5 ppm.

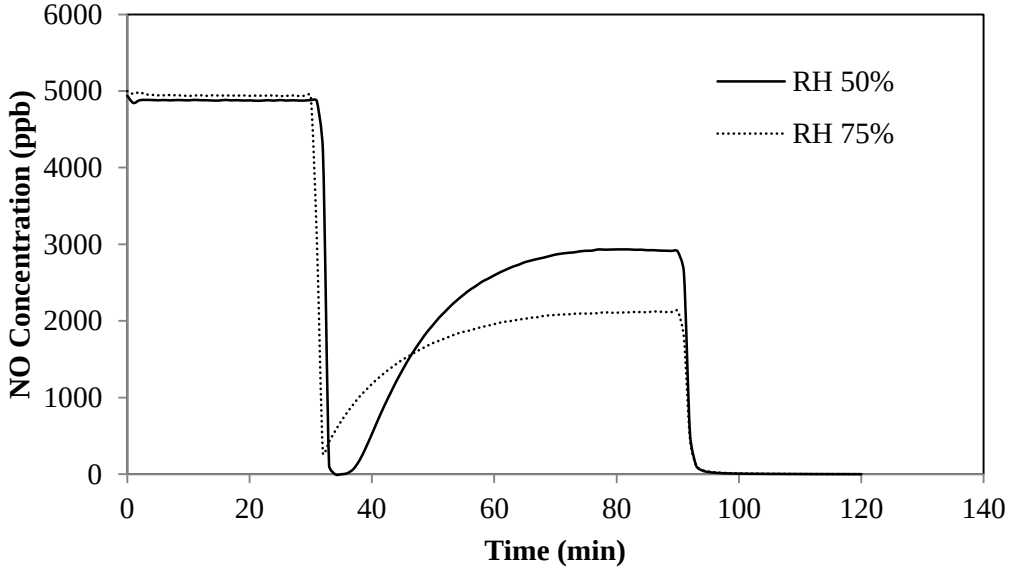

Figure 26. Effect of relative humidity for the same sample: TiO_2 loading is 0.63 g, inlet total flow rate is 1l/min, light intensity is 18.8 W/m^2, inlet NO concentration 5 ppm.

4.5.2 Mass Effect

The experiments with varying catalyst loadings were conducted. The results in Figure 27 showed that there was an optimum value for catalyst amount. Increasing catalyst amount on the glass increases the photocatalytic activity until a certain loading. After this value, degradation of NO was decreased due to agglomeration or higher opacity.

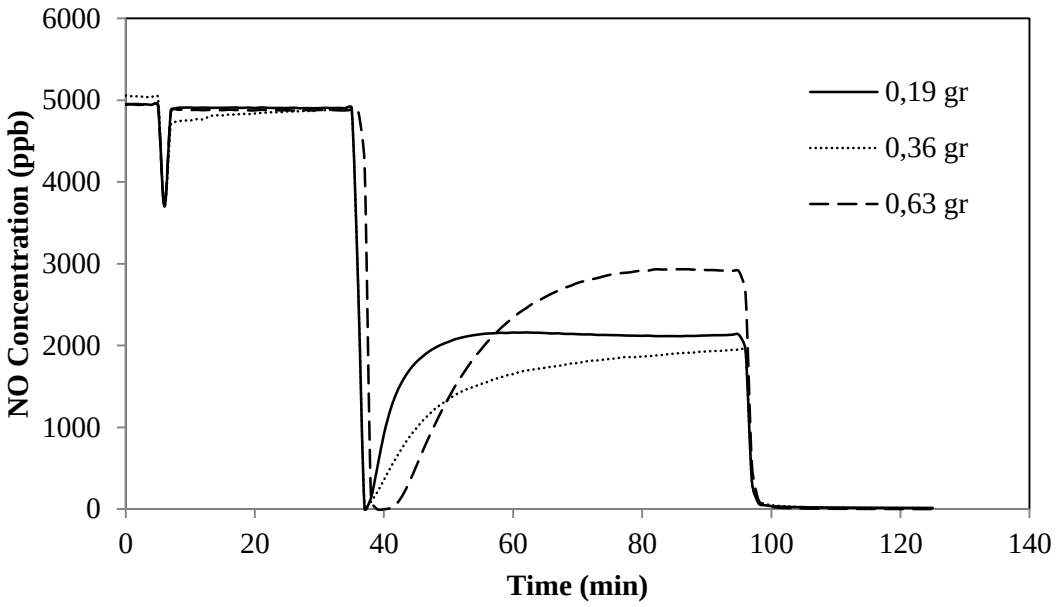

Figure 27. Mass effect on photocatalytic activity of the coated glass by doctor blade method: flow rate is 1l/min, light intensity is 18.8 W/m^2, inlet NO concentration 5 ppm.

4.5.3 Effect of Flow Rate

The aim of the experiment was to investigate effect of flow rate on the photocatalytic activity of NO_X. Three different flow rates were chosen as 1000 ml/min, 1500 ml/min and 2000

ml/min. Firstly, 2000 ml/min was sent to the reactor. Then, the flow rate was decreased. The inlet concentration was kept constant at 2500 ppb.

Two different coated glasses were prepared. They are loaded with 0.36 g TiO_2. Doctor blade method was only used for glass coating. One of the test pieces was cured at room conditions until the test piece is dried. It took approximately 24 hours. The other one was cured at furnace at 90^{o}C. It also took approximately 24 hours.

In Figure 28 and 29, the common thought is that the NO conversion is high at low flow rates. The reason is the higher residence time inside the reactor. After a certain flow rate, it is seen that the effect of the flow rate on the activity is similar. Since conversion decreases with increasing flow rate, we can say that we are in kinetically constrained regime. Drying sample in the furnace has negative effect at the low flow rate. At higher flow rates, similarity is observed.

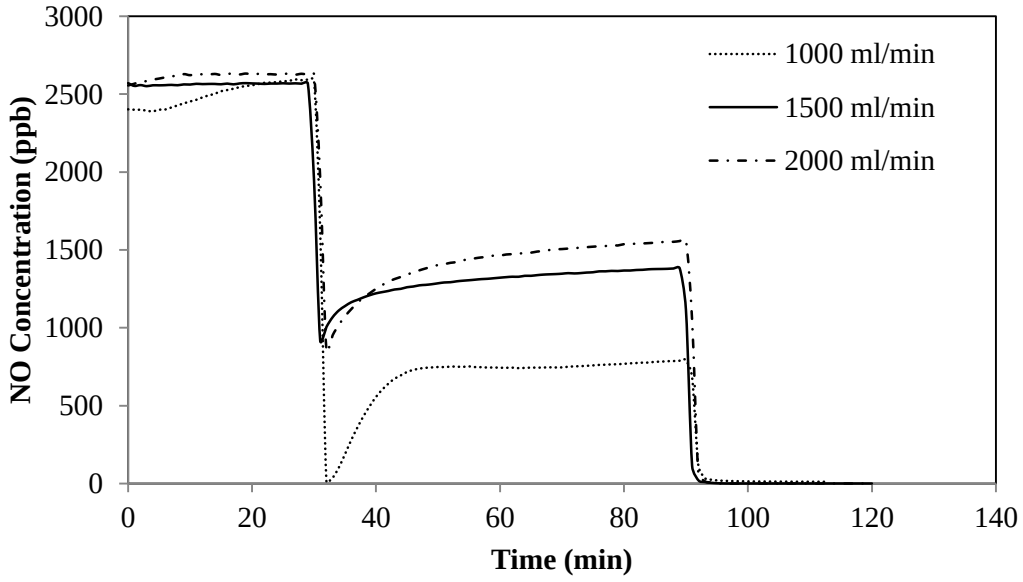

Figure 28. Effect of total flow rate on photocatalytic activity of the coated glass by doctor blade method: catalyst loading is 0.36 g, light intensity is 18.8 W/m^2, inlet NO concentration 5 ppm, it was cured at room conditions.

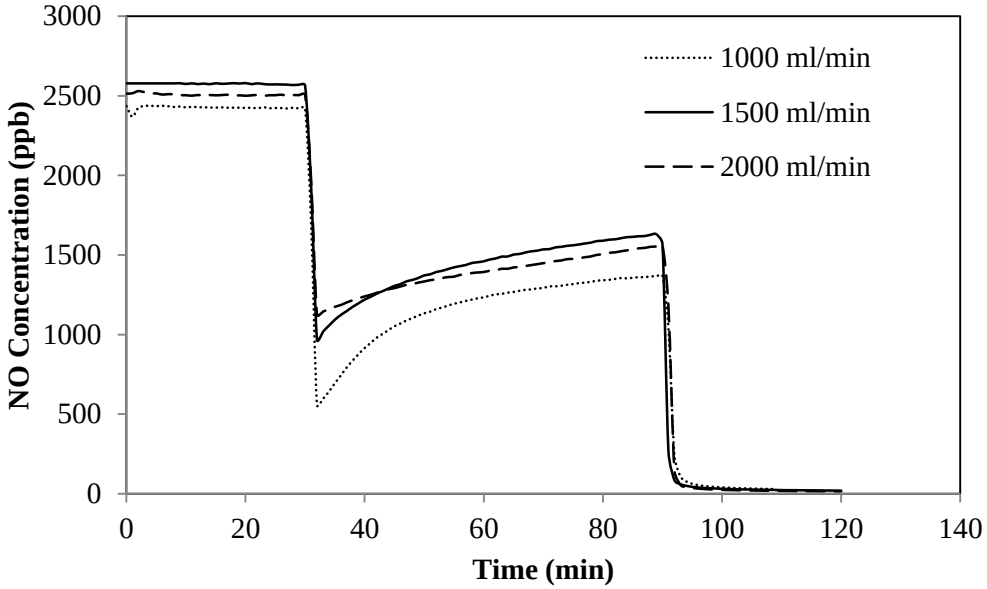

Figure 29. Effect of total flow rate on photocatalytic activity of the coated glass by doctor blade method: catalyst loading is 0.36 g, light intensity is 18.8 W/m^2, inlet NO concentration 5 ppm, it was cured at furnace.

4.5.4 Inlet Concentration

It is found that inlet NO concentration is one of the important factors in the literature survey. A glass was coated by doctor blade method. It was cured at room conditions until the test piece was dried. 0.36 g TiO_2 was loaded on the glass surface. The inlet concentrations were chosen as 1000 ppb, 2500 ppb and 5000 ppb. At first, higher concentration was sent to the reactor. Then, it was decreased. The results are represented in Figure 30. After an hour operation, the NO conversions are determined. The decrease on the conversion while increasing inlet concentration is shown in Figure 31.

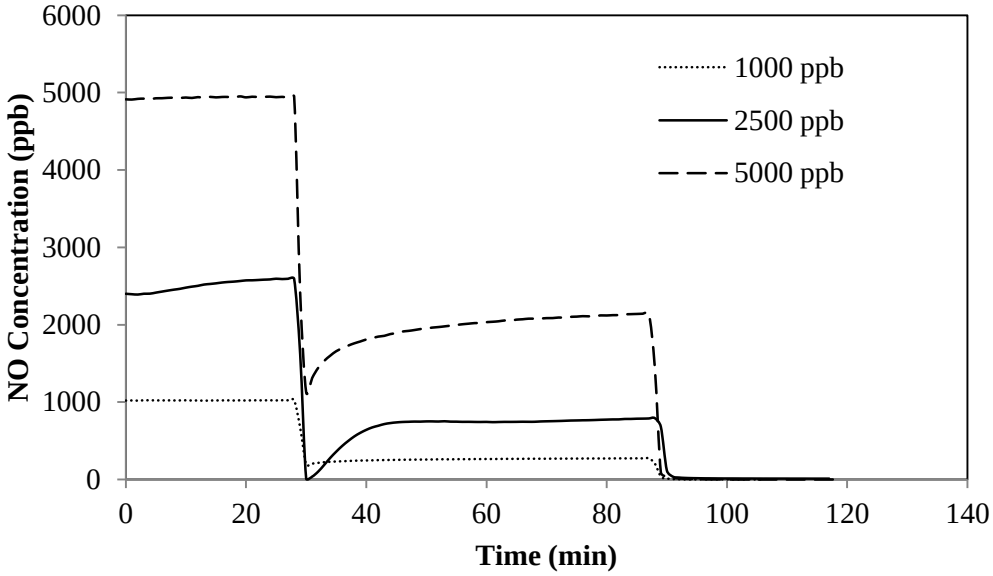

Figure 30. Effect of inlet concentration on the photocatalytic activity of the coated glass by doctor blade method: catalyst loading is 0.36 g, light intensity is 18.8 W/m^2, total flow rate is 1000 ml/min.

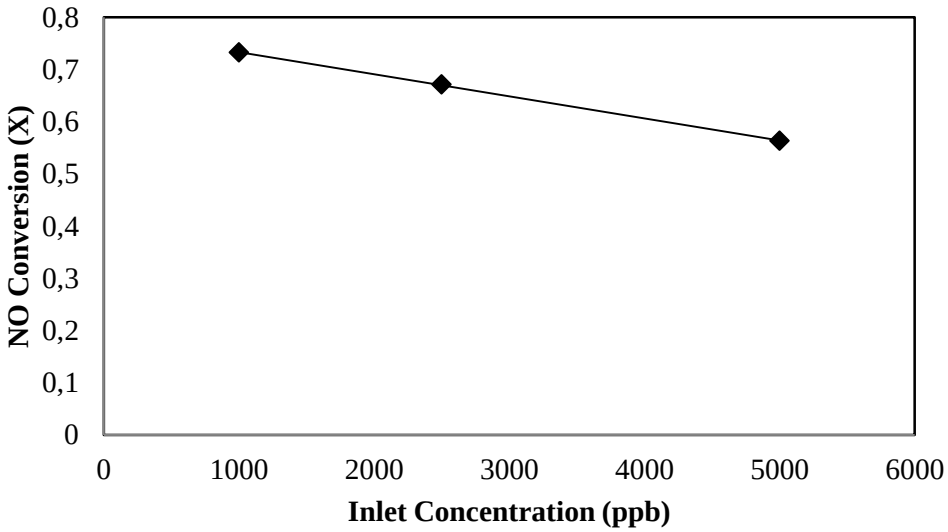

Figure 31. The effect of inlet NO concentration on the photocatalytic activity of the coated glass by doctor blade method: catalyst loading is 0.36 g, light intensity is 18.8 W/m^2, total flow rate is 1000 ml/min.

4.5. Heats of Hydration and Oxygen Adsorption by Microcalorimetry

In microcalorimetry measurements, the initial data for the differential heat of adsorption measurements were systematically higher. There are two adsorption states measured: a high energy site adsorbing water at ~80 kJ/mol. Another, lower heat of adsorption state was observed after a surface coverage of 300 μmol/g catalyst. The site energies were measured as ~40 kJ/mol on the average. The repeat experiments were shown with the empty symbols indicated repeatability in Figure 32 and 33.

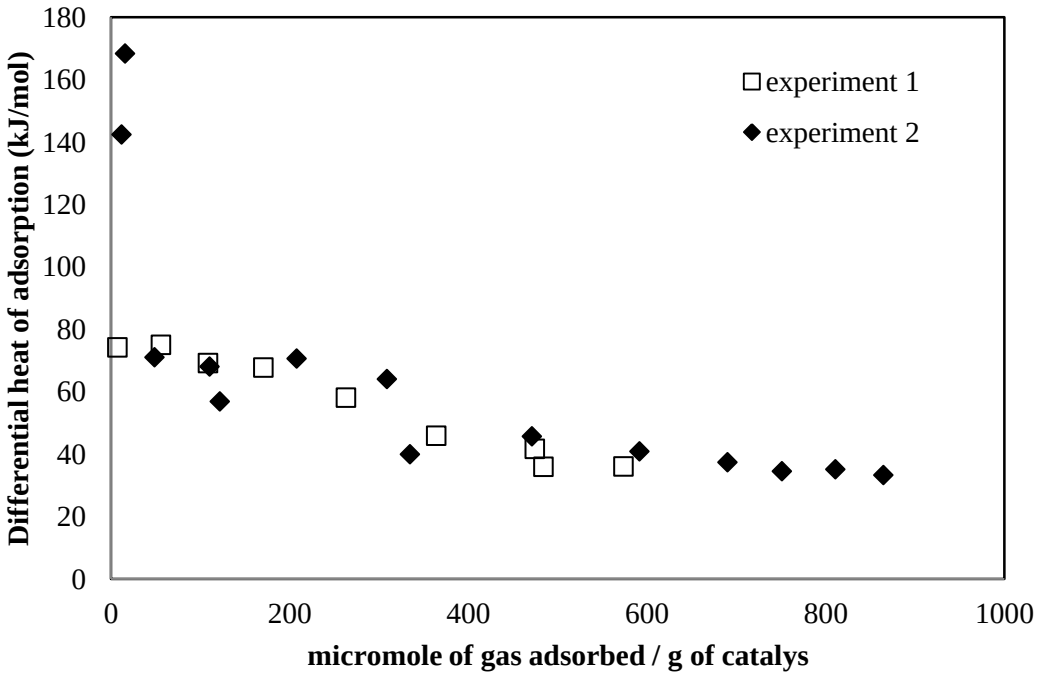

Figure 32. Differential heat of adsorption depends on the coverage.

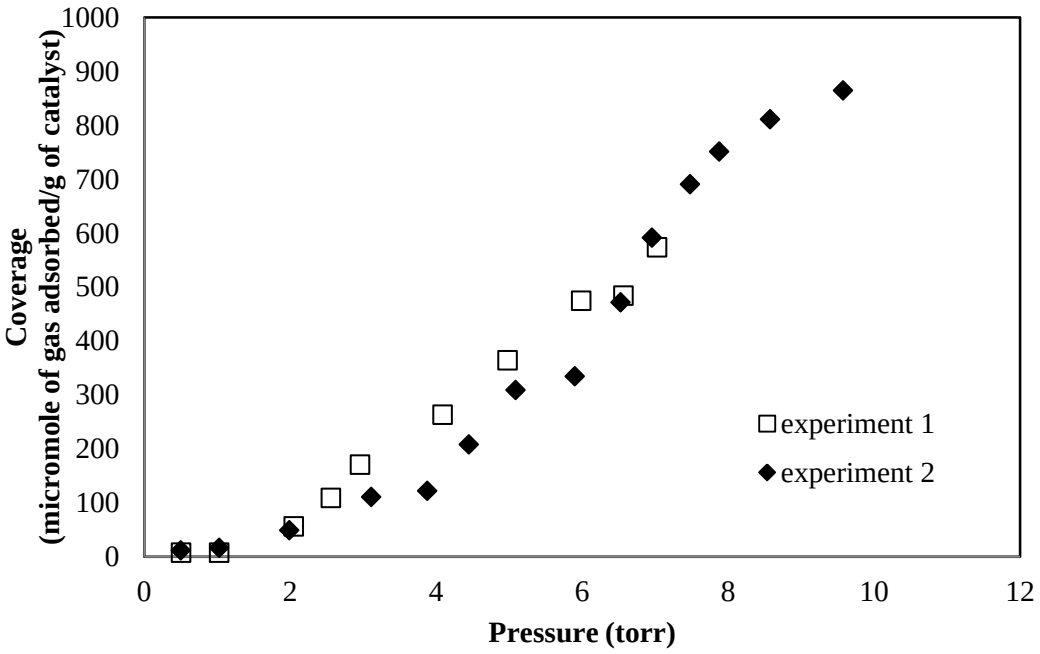

Figure 33. Pressure effect on the coverage.

In addition to measurement of heat of hydration, oxygen adsorption of TiO_2 was analyzed by microcalorimetry. It is observed that oxygen was not adsorbed by TiO_2 in Figure 34 and Figure 35. In Table 12, the pressure difference in the measurements was due to expansion of volume. The raw experimental data was shown in Appendix C.

Table 12. The pressure data at the beginning (P1), before the closing valve 3 (P2) at the end of experiment and after closing valve 3 (P3) at the end of experiment

Number	**P_1**	**P_2**	**P_3**
1	0,502	0,0437	0,0438
2	1,08	1,18	1,19
3	1,98	0,745	0,75
4	3,11	1,82	1,82
5	3,95	3,47	3,48
6	6,52	5,82	5,83

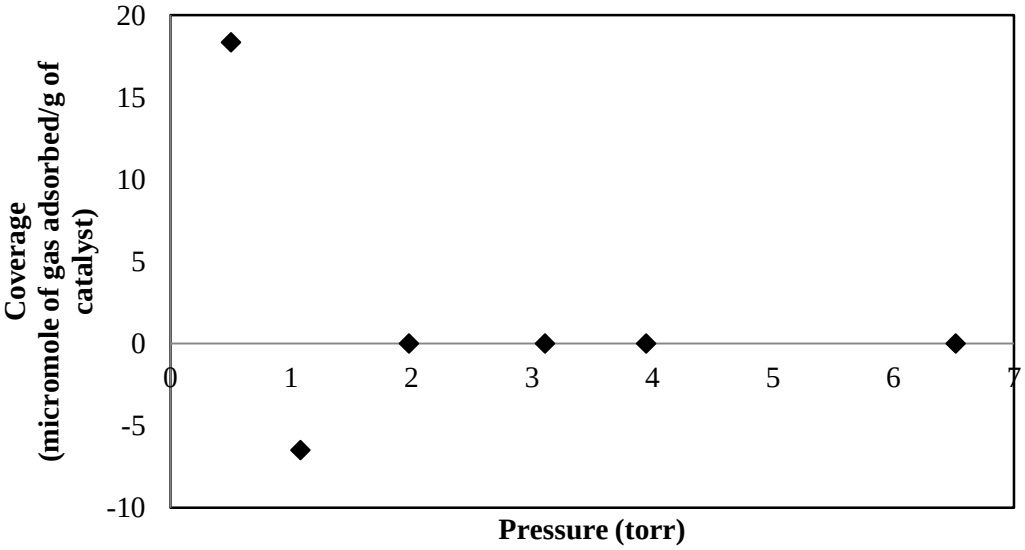

Figure 34. Oxygen coverage as a function of pressure over Degussa P25.

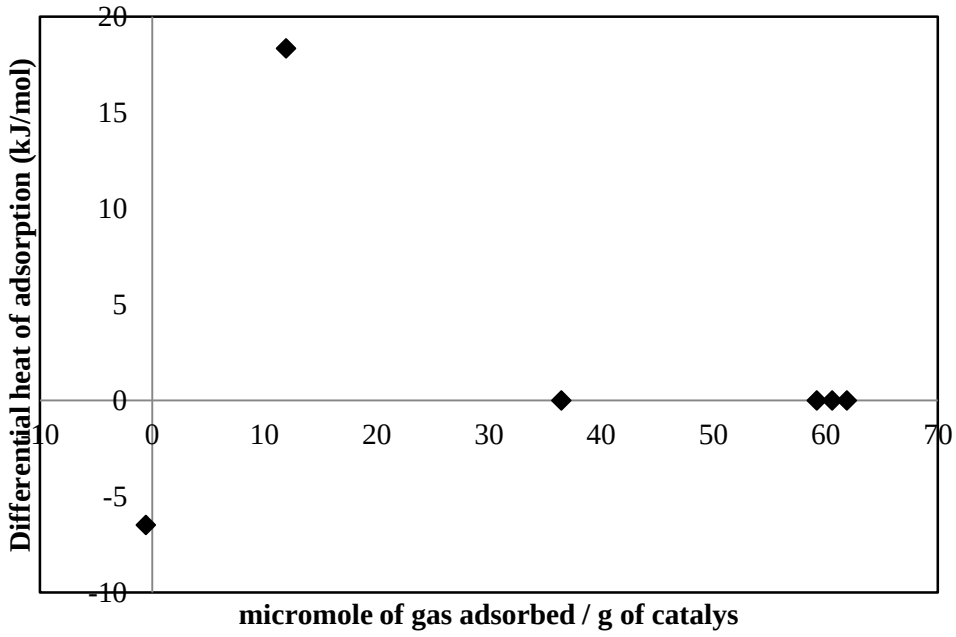

Figure 35. Differential heat of oxygen adsorption as a function of coverage.

4.6. Comment on Reaction Mechanism

From the results in Figure 36, it is understood that initial reaction rates are similar at different relative humidities.

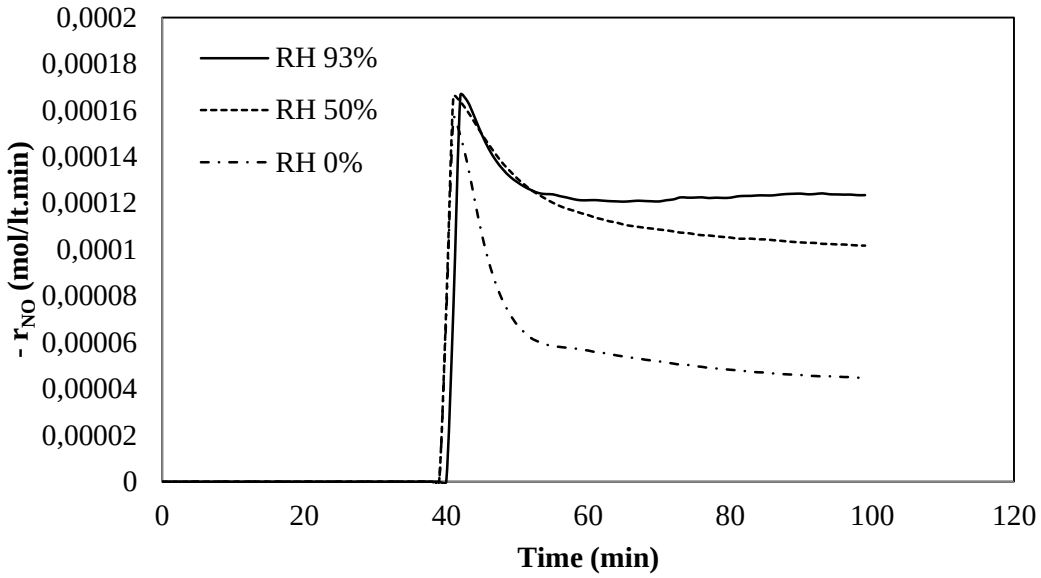

Figure 36. Reaction rate data for NO oxidation versus time data for different relative humidities: inlet total flow rate is 1l/min, light intensity is 18.8 W/m^2, inlet NO concentration 5 ppm.

The hydroxyl groups on the surface are dominant on reaction rate. Reaction rate data is calculated by the equation 1 for same time interval. Reaction rate for photocatalytic oxidation of NO describes the consumption amount of reactant as concentration per unit time. In the experiment, outlet concentration of NO_X is measured at the exit of the reactor by one minute periods. The inlet concentration is constant and known value. The difference between inlet and outlet concentration per unit time is calculated to determine reaction rate data. The rate was determined according to Eqn 4.1.

$$-r_{NO} = \frac{C_{NO_{in}} - C_{NO_{out}}}{dt} \qquad (4.1)$$

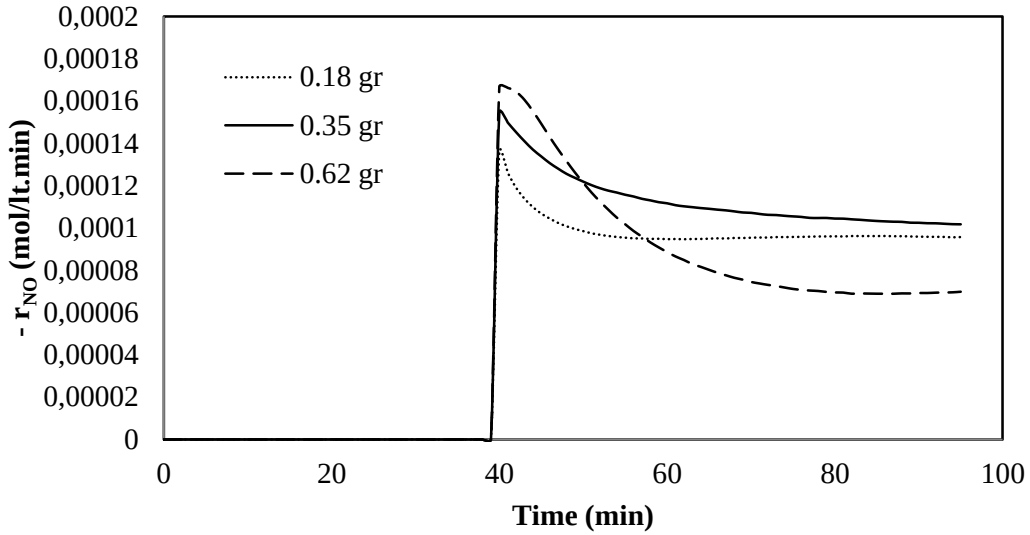

Figure 37. Reaction rate data for NO oxidation versus time data for different catalyst amount: inlet total flow rate is 1l/min, light intensity is 18.8 W/m^2, inlet NO concentration 5 ppm, relative humidity is 50%.

In Figure 37, the effect of the catalyst surface plays a vital role on reaction rate. Change on catalyst amount causes change on the surface of the catalyst. The total flow rate has also very effective role in Figure 38.

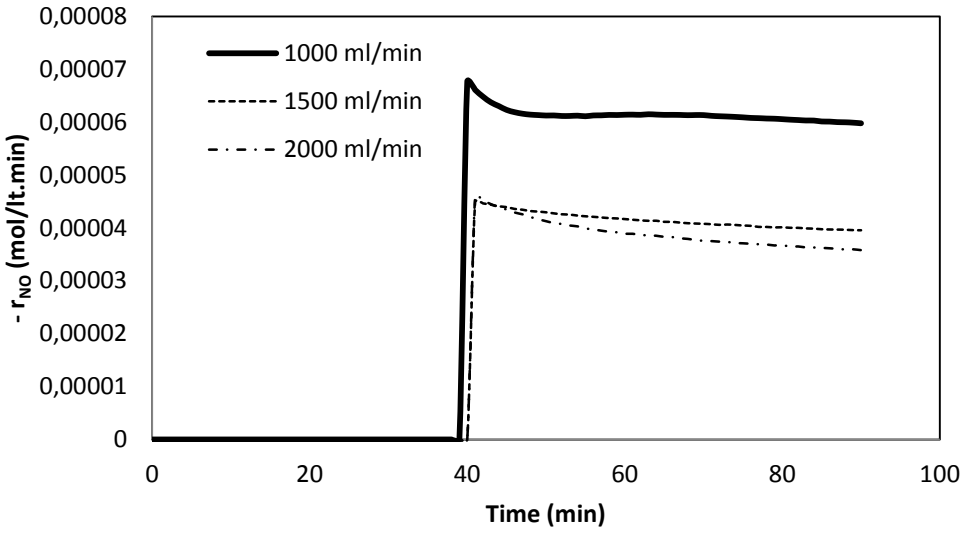

Figure 38. Reaction rate data for NO oxidation versus time data for different total flow rate: catalyst amount is 0.36 g, light intensity is 18.8 W/m^2, inlet NO concentration 2.5 ppm, relative humidity is 50%.

CHAPTER 5

SUMMARY AND CONCLUSIONS

In the scope of this thesis, a NO_X analysis test system based on ISO-22197:2007(E) standard that can monitor NO oxidation ability of photocatalytically active surfaces was constructed. The grout and glass surfaces showed similar photocatalytic activities in the experiments. Two types of coating method were achieved successfully, namely doctor blade method and sol-gel method. The photocatalytic activity of NO_x was observed in these coatings. In the light of ISO standard, the industrial samples given by Kalekim A.Ş. were tested. The fundamental tests showed that the home-built system works properly.

Kinetic studies were made on the surface of the glass coated by TiO_2. Effects of some parameters on the photocatalytic oxidation of NO_x were studied. These parameters were relative humidity, catalyst loading, total flow rate and inlet concentration. The results were discussed in detail. The similarity of the results with previous studies in this field was obtained. In addition, water and oxygen adsorption on TiO_2 surface was analyzed. The observation is that water adsorbs over TiO_2 surface at relatively high heats of adsorption (~80 kJ/mol) up to a monolayer coverage. After one monolayer the heat of adsorption decreases to ~40 kJ/mol. On the other hand, oxygen coverage was very low and no appreciable signal was detected for O_2. In addition to the reaction rate tests, the heat of adsorption measurements underlines the important role of water in photocatalytic oxidation processes.

REFERENCES

[1] Maggos, T., Bartzis, J.G., Leva, P., Kotzias, D., Application of photocatalytic technology for Nox removal, Appl. Phys. A, 89, 81-84, 2007

[2] Th Maggos, A. Plassais, J.G. Bartzis, Ch Vassilakos, N. Moussiopoulos, L Bonafous, (2008) Photocatalytic degradation of NOx in a pilot street canyon configuration using TiO2 mortal panels, Environ Monit Assess, 136:35–44

[3] A. Beeldens (2007) Air purification by road materials: results of the test project in Antwerp P. Baglioni, L. Cassar (Eds.), Proceedings international RILEM symposium on photocatalysis, environment and construction materials-TDP 2007, RILEM Publications, Bagneux, pp. 187–194

[4] G.L. Guerrini, E. Peccati (2007), Photocatalytic cementitious roads for depollution P. Baglioni, L. Cassar (Eds.), Proceedings international RILEM symposium on photocatalysis, environment and construction materials-TDP 2007, RILEM Publications, Bagneux, pp. 187–194

[5] Ogawa, Shinichiro, Air purification material and its use in air purification panel and exterior, panel,Jpn. Kokai Tokkyo Koho, 7 pp.

[6] Yasuoka, Kenji; Shimizu, Hiroshi;Itano, Naofumi; Aoki, Masaki; Sasaki, Shunsuke, Waterpermeable paved road having NOx removalfunction and its construction,JP 2004137842, A2, 20040513

[7] Horikirikawa, Kazuo; Yoshimura, Noriyuki; Hirose, Atsushi, Air purifying soundproof wall and its use,JP 2004011228, A2, 20040115

[8] Takami, Katsushige; Kono, Hitoshi, (2003), The measure against NOx using the photocatalytic materials along streets, Shokubai, 45(3), 241-246

[9] Kaneda, Yoshihisa; Sano, Kumiko;Ishimori, Masaki, Application of photocatalystimpregnated cement composition to surface finished outdoorstructuresthrough polymer mortar layer,JP 2003213610, A2, 20030730

[10] A. Folli (2010), TiO_2 Photocatalysis in Portland cement systems: Fundamentals of self cleaning effect and air pollution mitigation, Thesis, University of Aberdeen

[11] Hashimoto K, Irie H, Fujishima A (2005), TiO2 photocatalysis: a historical overview and future prospects, Japanese Journal of Applied PhysicsVol. 44, No. 12, pp. 8269–8285

[12] Linsebigler AL, Lu G, Yates JT Jr. (1995). Photocatalysis on TiO2 surfaces:principles, mechanisms, and selected results. Chem Rev.;95(3): 735–758

[13] Aaron Wold (1993), Photocatalytic properties of TiO_2, Chem. Mater. 5, 280-283

[14] Carp, O.; Huisman, C.L.; Reller, A.: Photoinduced reactivity of titanium dioxide, Progress in Solid State Chemistry (32), p. 33-177, 2004

[15] Dorian A. H. H., Charles C. S. (2011). Review of the anatase to rutile phase transformation, J Mater Sci (2011) 46:855–874

[16] Li, Y. and Ishigaki, T. (2002). Thermodynamic analysis of nucleation of anatase and rutile from TiO_2 melt, J. Cryst. Growth, 242, 511-516

[17] D.A.H. Hanaor, M.H.N. Assadi, S. Li, A. Yu, and C.C. Sorrell, (2012). Ab Initio Study of Phase Stability in Doped TiO_2 Computational Mechanics 50,(2) 185-194

[18] Herrmann, J. (1999). Heterogeneous photocatalysis: fundamentals and applications to the removal of various types aqueous pollutants. Catalysis Today, 53, pp.

[19] Hoffmann M. R., Martin S. T., Choi W. Y., Bahnemann D. W. (1995), Environmental Applications of Semiconductor Photocatalysis, Chem Rev, Vol. 95, No. 1., pp. 69-96

[20] Nitrogen Oxides (NOx), Why and How They Are Controlled, EPA 456/F-99-006R November 1999

[21] Dalton JS, Janes PA, Jones NG, Nicholson JA, Hallam KR, Allen GC. (2002) Photocatalytic oxidation of NOx gases using TiO2: a surface spectroscopic approach. Environ Pollut. 2002; 120(2):415-22.

[22] ISO-22197:2007(E) Standard

[23] D.M. Blake, Bibliography of Work on Photocatalytic Removal of Hazardous Compounds from Water and Air, NREL/TP-430-22197, National Renewable Energy Laboratory, Golden, 1997.

[24] Diebold U. (2003), The surface science of titanium dioxide, Surface Science Reports 48, 53-229

[25] Harada, H; Ueda, T. (1984), Photocatalytic activity of ultra-fine rutile in methanol-water solution and dependence of activity on particle size, Chem. Phys. Lett., 106, 229

[26] K.Skalska, J.S. Miller, S.Ledakowicz: Trends in NOx abatement a review. Total Science of Environment, 2010, 1-2, 125-130

[27] S. Salasc, M. Skoglundh, and E. Fridell (2002), A comparison between Pt and Pd in NOx storage catalysts, Applied Catalysis B-Environmental, 36, 145

[28] F. Rohr, U. Göbel, P. Kattwinkel, T. Kreuzer, W. Müller, S. Philipp, P. Gélin (2007), New insight into the interaction of sulfur with diesel NOx storage catalysts, Appl. Catal. B: Environmental 70, 189–197

[29] F. Garin, (2004) Environmental catalysis. Catal. Today, 89 (3), 255–268

[30] H.Y. Huang, R.Q. Long, R.T. Yang. (2001), A highly sulfur resistant Pt-Rh/TiO_2/Al_2O_3 storage catalyst for NO x reduction under lean-rich cycles, Applied Catalysis B: Environmental 33, 127–136

[31] A. Pietraszek, P. Da Costa, R. Marques, P. Kornelak, T.W. Hansen, J. Camra, M. Najbar (2007), The effect of the Rh–Al, Pt–Al and Pt–Rh–Al surface alloys on NO conversion to N_2 on alumina supported Rh, Pt and Pt–Rh catalysts, Catalysis Today, Volume 119, Issues 1–4, Pages 187-193

[32] H. Yoneyama, N. Nishimura, and H. Tamura, J. Phys. Chem., 85, 268 (1981)

[33] Hori Y., A. Nakatsu & S. Suzuki, 1985. Heterogeneous photocatalytic oxidation of NO_2^- in aqueous suspension of various semiconductor powders. Chem. Lett., 1429–1432.

[34] Ibusuki T.; Takeuchi K. (1994), Removal of low concentration nitrogen oxides through photoassisted heterogeneous catalysis, Journal of molecular catalysis, Volume 88, Issue 1, Pages 93-102

[35] M. E. Simonsen, Z. Li, and E. G. Søgaard, "Influence of the OH groups on the photocatalytic activity and photoinduced hydrophilicity of microwave assisted sol-gel TiO_2 film," Applied Surface Science, vol. 255, no. 18, pp. 8054–8062, 2009.

[36] Devahasdin S, Fan C. Li JK, and Chen DH (2003). TiO2 photocatalytic oxidation of nitric oxide: transient behavior and reaction kinetics. Journal of Photochemistry and Photobiology A: Chemistry 156: 161-170.

[37] Wang, H.; Wu Zhongbiao W.; Zhao W.; Guan B.,(2007), Photocatalytic oxidation of nitrogen oxides using TiO_2 loading onwoven glass fabric, Chemosphere 66 185-190

[38] Yin S.; Liu B.; Zhang P.; Morikawa T.; Yamanaka K.; Sato T. (2008), Photocatalytic oxidation of NO_x under visible LED light irradiation over Nitrogen-Doped titania particles with iron or platinum loading, J. Phys. Chem. C, 112, 12425-12431

[39] Yu, Q.L., Brouwers, H.J.H. (2009) Indoor air purification using heterogeneous photocatalytic oxidation. Part I: Experimental study. Applied Catalysis B: Environmental 92, 454-461

[40] G. Hüsken, M. Hunger, H.J.H. Brouwers, Experimental study of photocatalytic concrete products for air purification, Build. Environ. 44 (2009) 2463–2474.

[41] Hunger, M., G. Husken, H.J.H. Brouwers, 2010. Photocatalytic degradation of air pollutants — From modeling to large scale application, Cement and Concrete Research, 40: 313-320.

[42] Martinez T, Bertron A, Ringot E, Escadeillas G (2011). Degradation of NO using photocatalytic coatings applied to different substrates. Building and Environment. 46: 1808-1816.

[43] João V. Staub de Melo, Glicério Trichês (2012) Evaluation of the influence of environmental conditions on the efficiency of photocatalytic coatings in the degradation of nitrogen oxides (NOx) Building and Environment, Volume 49, Pages 117-123

[44] H. Tawara, et al., Development of evaluation method of air-purifying paving blocks for NO x removal capacity, in: Proceedings of the Fourth International Conference on TiO 2 Photocatalytic Purification and Treatment of Water and Air, Albuquerque, NM, 24–28 May 1999.

[45] Inel, Yuksel; Okte, Ayse Neren, Photocatalytic degradation of malonic acid in aqueous suspensions of titanium dioxide: an initial kinetic investigation of CO_2 photogeneration, Journal of Photochemistry and Photobiology A: Chemistry, 1996, 96(1-3), 175-180

[46] Assabane, A; Ichou, YA; Tahiri, H; Guillard, C; Herrmann, JM, Photocatalytic degradation of polycarboxylic benzoic acids in UV-irradiated aqueous suspensions of Titania. Identification of intermediates and reaction pathway of the photomineralization of trimellitic acid (1,2,4-benzene tricarboxylic acid), APP CATAL B, 24(2), 2000, pp. 71-87

[47] D. Chen and A. K. Ray, "Photocatalytic Kinetics of Phenol and Its Derivatives over UV Irradiated TiO2," Applied Catalysis B: Environmental, Vol. 23, No. 2-3, 1999, pp. 143-157. doi:10.1016/S0926-3373(99)00068-5

[48] Toma, F.L., Bertrand, G., Klein, D., et al. (2004) Photocatalytic removal of nitrogen oxides via titanium dioxide. Environmental Chemistry Letters, 2, 117-121

[49] C.H. Ao, S.C. Lee, Appl. Catal. B: Environ. 44 (2003) 191–205

[50] Q. L. Yu, M. M. Ballari, H. J. H. Brouwers. Applied Indoor air purification using heterogeneous photocatalytic oxidation. Part II: Kinetic study. Appl Catal B 99:8 (2010)

[51] Kemmitt, T., Al-Salim N. I., Lian J.,Golovko V. B., and Ruzicka J. - Y. (2013),Transparent, photocatalytic, titania thin films formed at low temperature, Current Applied Physics, Volume 13, Number 1, p.142-147.

[52] Zhu J., Yang J., Bian Z.-F., Ren J., Liu Y.-M., Cao Y., Li H.-X., He H.-Y., Fan K.-N. (2007) Nanocrystalline anatase TiO2 photocatalysts prepared via a facile low temperature nonhydrolytic sol-gel reaction of TiCl4 and benzyl alcohol, Applied Catalysis B: Environmental, 76 (1-2) , pp. 82-91

[53] Brinker, M.S. Harrington, 1981, Solad Energy Mater. S, pp 159

[54] V. Anand Ganesh, A. Sreekumaran Nair, H. K. Raut, T. M. Walsh, and S. Ramakrishna,(2011). Photocatalytic Superhydrophilic TiO2 Coating on Glass by Electrospinning, RSC Advances, 2012, 2, 2067–2072

[55] Celik E, Keskin I, Kayatekin I, Ak Azem F and Özkan E. Al2O3–TiO2 thin films on glass substrate by sol–gel technique. Materials Characterization, 2007; 58: 349 – 357.

[56] Hornbeck J. H. (1999), Restoration and Reclamation Review, Vol. 5. No:1

[57] Luiz D. B., Andersen S. L. F., Berger C., José H. J., Moreira R. F. P. M. (2012), Photocatalytic reduction of nitrate ions in water over metal-modified TiO_2, Journal of Photochemistry and Photobiology A: Chemistry 246, 36-44

[58] Pirkanniemi K. and Sillanpaa M. (2002) Heterogeneous water phase catalysis as an environmental application: a review, Chemosphere, 48, 1047-1060

[59] Anderson J. A. (2011), Catalysis Today 175 316– 321

[60] M. M. Oymak's Ph.D. Thesis (2013). Middle East Technical University, Turkey

[61] D. Uner, N.A. Tapan, I. Ozen, M. Uner (2003) Oxygen adsorption on Pt/TiO_2 catalysts, Appl. Catal. A: Gen., 251, pp. 225–234

[62]]R. Krahnert, Ammonia Oxidation over Polycrystalline Platinum: Surface Morphology and Kinetics at Atmospheric Pressure, Technical University of Berlin, 2005

[63] F. Kuhlmann, Liebigs Ann. Chem., 29 (1839) 272

[64] V.A Sadykov, L.A Isupova, I.A Zolotarskii, L.N Bobrova, A.S Noskov, V.N Parmon, E.A Brushtein, T.V Telyatnikova, V.I Chernyshev, V.V Lunin, Applied Catalysis A: General 204 (2000) 59–87

[65] L. S. Benner, T. Suzuki, K. Meguro and S. Tanaka, "Precious Metals Science and Technology", based on Kikinzoku no Kagaku, the 100th Anniversary Commemorative Publ. of Tanaka Kikinzoku Kogyo K. K., Japan, International Precious Metals Institute, 1991

[66] D.A. Hickman, M. Huff, L.D. Schmidt, Ind. Eng. Chem. Res. 1993,32,809-817

[67] B.X. Hu, Y. Ning, L. Chen, Q. Shi and C. Jia, Platinum Metals Rev., 2012, 56, (1), 40–46
[68] F. Sperner, W. Hohmann, Platinum Metals Rev. 20 (1976) 12
[69] C.M. Hung, W.L. Lai,and J.L. Lin, Aerosol and Air Quality Research, 12: 583–591, 2012
[70] M. Asscher, W. L. Guthrie, T.-H. Lin, and G. A. Somorjai, The Journal of Physical Chemistry, Vol. 88, No. 15, 1984
[71] R. Kraehnert , M. Baerns, Chemical Engineering Journal 137 (2008) 361–375
[72] E. V. Rebrov, M. H. J. M. de Croon and J. C. Schouten, Chem. Eng. Res. Design 81 (2003) 744
[73] A. Scheibe, U. Lins, R. Imbihl, Surf. Sci. 577 (2005) 1
[74] Dean, John A. Lange's Handbook of Chemistry, 15th ed.; McGraw-Hill Book Company: New York, NY, 1998; p 6.104

APPENDIX A

CALIBRATION OF CHEMILUMINESCENCE NO-NO_2-NO_x ANALYZER

The calibration procedure is applied for the Chemiluminescence NO-NO_2-NO_x analyzer which is the Model 42i. This procedure is written in the manual of the analyzer. Calibration is divided into three main parts. Firstly, pre-calibration is performed before calibration procedure. In this procedure, Instrument is allowed to warm up and stabilize. Ozonator is turn on. Instrument is operated in the auto mode. NO, NO_2 and NO_X ranges are determined. The averaging time to show data on the screen is adjusted. The averaging time should be less than the zero duration and span duration. Secondly, the following procedure is calibration. It contains three stages; setting the NO and NO_X background to zero, calibrating the NO channel to the NO calibration gas and calibrating the NO_X channel to the NO_X calibration gas Standard gas is supplied to the system. All NO and NO_X values are equalized to zero. Then, the calibration gas of which the concentration is known is sent to the analyzer. The NO and NO_x channels are adjusted according to this gas. At the final, the concentration of calibration gas is decreased to a known value. The values on the screen are controlled whether it is correct or not. At least three points can be enough to check the analyzer.

APPENDIX B

This appendix is added in order to provide sufficient background in thermal NO oxidation mechanisms. The most studied of these mechanisms belongs to ammonia oxidation literature. Therefore, a brief literature survey and the relevant mechanisms are presented here.

AMMONIA OXIDATION

Nitric acid production is one of the most important processes in worldwide. It is the intermediate material of the fertilizer. The annual world capacity was about 50 Mt HNO_3 in 2005 [62]. Platinum-catalyzed ammonia oxidation was secured by patent in 1839 [63]. The use of production of nitric acid as an industrial application began with the Ostwald's research about the development of this process [64]. He patented this process in 1902. A Pt-Rh alloy containing 92.5-93% Pt and 7.0-7.5% Rh was patented by Dupont in the 1940s [65]. The Ostwald process contains three major steps. The first step is the oxidation of ammonia by air to yield nitric oxide over Pt or Pt-Rh gauze catalysts. NO is the main product of this step and N_2O and N_2 are the by-products. The second step is the gas-phase oxidation of NO to NO_2. The third step is the absorption of NO_2 in water to form HNO_3 [62,64,66]. The efficiency of the ammonia oxidation is the most focused part in this process, because 90% of the nitric acid production cost usually depends on ammonia [64,67].

Catalyst development for NH_3 oxidation started with pure platinum gauzes at the beginning of the 19th century. Platinum-rhodium alloys took the place of pure platinum gauzes. Rhodium content in these alloys varied from 5 to 10%. There has been many research to develop catalyst activity [67]. Platinum-palladium-rhodium alloys have been used as the main catalysts nowadays due to nitric acid production cost [64,67]. Optimum operating data for ammonia oxidation is shown in Table B1.

Table B 1. Optimum operating data for ammonia combustion [68]

Pressure	Gauze temperature (^oC)	NH_3 content (vol.%)	Yield (%)	Pt loss (g/t HNO_3)	Operating time (months)
Atmospheric	810-850	12.0-12.5	97.0-98.0	0.04-0.05	8-12
Medium 3-5 atm	870-890	10.5-11.0	96.5-96.5	0.10-0.11	4-6
High 7-9 atm	920-940	10.3-10.5	94.5-95.0	0.25-0.30	1.5-3

Hung et al. [69] determined that nearly 100% of the NH_3 was oxidized over Pt-Rh binary catalyst at 673 K and oxygen content of 4%. It was found that the main product is N_2.

To improve catalytic activity, kinetics studies have been conducted by many researchers. Sadykov et al. [64] gave a perspective to main factors determining performance of precious metals and oxides in the high-temperature ammonia oxidation by generalizing the research and development of industrial oxide catalysts for ammonia oxidation in the nitric acid production within two-bed technology of the high pressure process.

Asscher et al. [70] determined that there are at least two competing mechanism for the oxidation of ammonia on a Pt(111) single-crystal surface ; (1) a surface reaction between adsorbed atomic oxygen and nitrogen, (2) a surface mechanism between oxygen and an NH fragment in which the desorption of NO is the rate-limiting step.

Kraehnert [71] investigated the reaction kinetics and changes on the Pt catalyst for oxidation of ammonia in his PhD thesis. It is made a kinetic model to lighten the ammonia oxidation process.

Hu et al. [67] studied physical properties and application performance of Platinum-Palladium-Rhodium alloys modified with cerium. It was reported that the Pt-4Pd-3.5Rh-0.1Ce alloy show higher conversion rate for the ammonia oxidation to NO, better resistance to corrosion, adhesion and poisoning, a lower Pt loss rate and longer service life for the production of nitric acid in industrial atmospheric and medium pressure reactors.

There are different reaction mechanisms of ammonia oxidation with respect to many studies. These different approaches to the reaction mechanism of ammonia oxidation are sourced by the different kinetic models. Reaction mechanisms can clarify the influence of catalyst pretreatment on catalyst activity, the activation/deactivation behavior and the product distribution [62]. Rebrov et al. [72] used an aluminum-based microstructured reactor/heat exchanger and obtain the reaction scheme with respect to lumped reaction model in Table B2.

Table B 2. Lumped reaction models for ammonia oxidation on a Pt catalyst [72]

No	Model A: on-top and bridge sites are equivalent	Model B: hollow and bridge sites are equivalent
L1	$NH_3 + \{\ \} \rightarrow \{NH_3\}$	$NH_3 + \{\ \} \rightarrow \{NH_3\}$
L2	$\{NH_3\} \rightarrow NH_3 + \{\ \}$	$\{NH_3\} \rightarrow NH_3 + \{\ \}$
L3	$O_2 + 2(\ ) \rightarrow 2(O)$	$O_2 + 2(\ ) \rightarrow 2(O)$
L4	$(O) + (O) \rightarrow O_2 + 2(\ )$	$(O) + (O) \rightarrow O_2 + 2(\ )$

L5	$\{NH_3\} + 3(O) \rightarrow \{N\} + 3(OH)$	$\{NH_3\} + 3(O) + (\ ) \rightarrow (N) + 3(OH) + \{\ \}$
L6	$\{N\} + \{N\} \rightarrow N_2 + 2\{\ \}$	$(N) + (N) \rightarrow N_2 + 2(\ )$
L7	$\{N\} + \{NO\} \rightarrow N_2O + 2\ \{\ \}$	$(N) + \{NO\} \rightarrow N_2O + (\ ) + \{\ \}$
L8	$\{NO\} + (\ ) \rightarrow \{N\} + (O)$	$\{NO\} + 2(\ ) \rightarrow (N) + (O) + \{\ \}$
L9	$(OH) + (OH) \rightarrow (O) + (\ ) + H_2O$	$(OH) + (OH) \rightarrow (O) + (\ ) + H_2O$
L10	$\{N\} + (O) \rightarrow \{NO\} + (\ )$	$(N) + (O) + \{\ \} \rightarrow \{NO\} + (\ ) + (\ )$
L11	$H_2O + (\ ) + (O) \rightarrow (OH) + (OH)$	$H_2O + (\ ) + (O) \rightarrow (OH) + (OH)$
L12	$\{NO\} \rightarrow NO + \{\ \}$	$\{NO\} \rightarrow NO + \{\ \}$
L13	$N_2O + (\ ) \rightarrow N_2 + (O)$	$N_2O + (\ ) \rightarrow N_2 + (O)$

The conditions for which model A is valid, are as follows: NH_3 partial pressure, 0.01-0.12 atm; O_2 partial pressure, 0.10-0.88 atm; temperature, 130-325^oC; contact time, 0.3-0.7 ms; sites 1, { }; sites 2, ( ).
The conditions for which model B is valid, are as follows: NH_3 partial pressure, 0.03-0.20 atm; O_2 partial pressure, 0.10-0.88 atm; temperature, 130-400^oC; contact time, 0.3-0.7 ms.

Scheibe et al. [73] studied the kinetics of ammonia oxidation with oxygen at low pressures with respect to Rebrov et al. [72] because it was thought that there are mass transport limitations on the conversion rate at high pressures. Scheibe et al. [73] suggested the reaction pathways in Table B3.

Table B 3. Reaction pathways for ammonia oxidation [73]

No	Reactions	
R1	$NH_{3,ad} \rightarrow N_{ad} + 3H_{ad}$	dissociation of ammonia
R2	$O_2 + 2* \leftrightarrow 2O_{ad}$	dominant reaction pathway is direct hydrogen abstraction by chemisorbed oxygen or OH species
R3	$NH_3 + * \leftrightarrow NH_{3,ad}$	
R4	$NH_{3,ad} + O_{ad} \leftrightarrow NH_{2,ad} + OH_{ad}$	
R5	$NH_{2,ad} + O_{ad} \leftrightarrow NH_{ad} + OH_{ad}$	
R6	$NH_{ad} + O_{ad} \leftrightarrow N_{ad} + OH_{ad}$	
R7	$NH_{3,ad} + OH_{ad} \leftrightarrow NH_{2,ad} + H_2O + *$	
R8	$NH_{2,ad} + OH_{ad} \leftrightarrow NH_{ad} + H_2O + *$	
R9	$NH_{ad} + OH_{ad} \leftrightarrow N_{ad} + H_2O + *$	
R10	$2N_{ad} \rightarrow N_2 + 2*$	
R11	$N_{ad} + O_{ad} \leftrightarrow NO_{ad} + *$	
R12	$NO_{ad} \rightarrow NO + *$	
R13	$O_{ad} + H_{ad} \leftrightarrow OH_{ad}$	
R14	$OH_{ad} + H_{ad} \rightarrow H_2O + 2*$	
R15	$2OH_{ad} \leftrightarrow O_{ad} + H_2O$	
R16	$NO_{ad} + O_{ad} \rightarrow N_2O + 2*$	N_2O formation which was not observed at low pressures below 10^{-3} mbar
R17	$2NO_{ad} \rightarrow N_2O + O_{ad} + *$	

Asterisk * refers to a vacant adsorption site

Kraehnert et al. [71] developed these two models and determined a best-fitting kinetic model for ammonia oxidation. The polycrystalline Pt catalyst was used. The temperature of process was between 286 and 385^{o}C. Reactant partial pressures were between 1 and 6 kPa. Reactions were presented in Table B4.

Table B 4. Reactions for ammonia oxidation [71]

No	Reactions
R1	$NH_3 + b \leftrightarrow NH_3\text{-}b$
R2	$O_2 + 2a \leftrightarrow 2O\text{-}a$
R3	$NH_3\text{-}b + (3/2)O\text{-}a \rightarrow N\text{-}a + (3/2)H_2O + (1/2)a + b$
R4	$NO\text{-}a \leftrightarrow NO + a$
R5	$2N\text{-}a \rightarrow N_2 + 2a$
R6	$N\text{-}a + O\text{-}a \rightarrow NO\text{-}a + a$
R7	$NO\text{-}a + N\text{-}a \rightarrow N_2O + 2a$

Adsorption sites-(a) O, N, NO; (b) NH_3

APPENDIX C

RESULTS OF HEAT OF HYDRATION AND OXYGEN ADSORPTION BY MICROCALORIMETRY

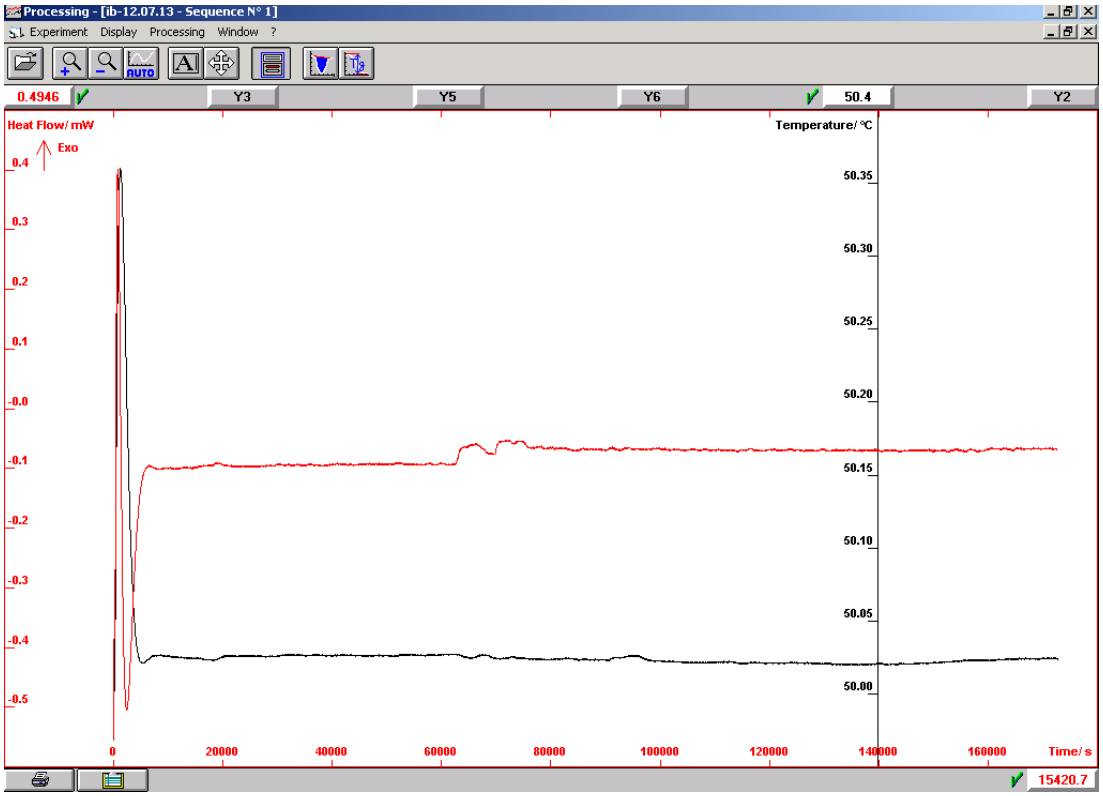

Figure C 1. Microcalorimetry experiments results for oxygen adsorption

Table C 1. Raw data of second experiment for heats of hydration by Microcalorimetry

							Incremental	Cumulative	Cum. N_{ads}/ $g_{catalyst}$	Inc. N_{ads}/ $gr_{catalyst}$	Heat	Heat/N_{ads}
Number	P_1	P_2	P_3	N_1	N_2	N_{cell}	N_{ads}	N_{ads}	[µmole/$g_{catalyst}$]	[mole/$g_{catalyst}$]	(j/g_{cat})	(kj/mol)
1	0,5	0,0496	0,05	6,74E-06	8,80E-07	2,14E-07	5,865E-06	5,865E-06	11,730	1,173E-05	1,6711	142,46
2	1,03	0,672	0,674	1,38E-05	1,19E-05	2,91E-06	2,128E-06	7,993E-06	15,986	4,256E-06	0,7163	168,31
3	1,99	0,745	0,75	2,67E-05	1,32E-05	3,23E-06	1,642E-05	2,442E-05	48,831	3,285E-05	2,3323	71,01
4	3,11	0,803	0,807	4,17E-05	1,43E-05	3,48E-06	3,077E-05	5,519E-05	110,372	6,154E-05	4,1895	68,07
5	3,88	2,81	2,82	5,21E-05	4,99E-05	1,22E-05	5,743E-06	6,093E-05	121,858	1,149E-05	0,6528	56,83
6	4,45	1,63	1,64	5,97E-05	2,89E-05	7,07E-06	4,302E-05	1,040E-04	207,901	8,604E-05	6,0742	70,59
7	5,09	1,4	1,41	6,83E-05	2,48E-05	6,08E-06	5,062E-05	1,546E-04	309,134	1,012E-04	6,4856	64,06
8	5,9	4,09	4,1	7,92E-05	7,25E-05	1,77E-05	1,277E-05	1,673E-04	334,670	2,554E-05	1,0203	39,95
9	6,53	2,09	2,1	8,77E-05	3,71E-05	9,05E-06	6,832E-05	2,357E-04	471,318	1,366E-04	6,2392	45,65
10	6,96	2,39	2,39	9,35E-05	4,24E-05	1,03E-05	6,016E-05	2,958E-04	591,630	1,203E-04	4,9184	40,88
11	7,48	3,46	3,47	1,01E-04	6,14E-05	1,49E-05	4,940E-05	3,452E-04	690,437	9,881E-05	3,6924	37,37
12	7,88	5,1	5,11	1,06E-04	9,05E-05	2,20E-05	3,033E-05	3,755E-04	751,093	6,066E-05	2,0958	34,55
13	8,58	6,05	6,06	1,15E-04	1,07E-04	2,61E-05	2,994E-05	4,055E-04	810,979	5,989E-05	2,107	35,18
14	9,58	7,21	7,23	1,29E-04	1,28E-04	3,12E-05	2,689E-05	4,324E-04	864,755	5,378E-05	1,7897	33,28

Table C 2. Raw data of first experiment for heats of hydration by Microcalorimetry

							Incremental	Cumulative	Cum. N_{ads}/ $g_{catalyst}$	Inc. N_{ads}/ $gr_{catalyst}$	Heat	Heat/N_{ads}
Number	**P_1**	**P_2**	**P_3**	**N_1**	**N_2**	**N_{cell}**	**N_{ads}**	**N_{ads}**	**[µmole/$g_{catalyst}$]**	**[mole/$g_{catalyst}$]**	**(j/gcat)**	**(kj/mol)**
1	0,504	0,18	0,181	6,77E-06	3,19E-06	7,80E-07	3,578E-06	3,578E-06	7,155	7,155E-06	0,5312	74,24
2	1,03	0,818	0,821	1,38E-05	1,45E-05	3,53E-06	1,027E-07	3,680E-06	7,361	2,054E-07	0,218	1061,16
3	2,05	0,382	0,384	2,75E-05	6,78E-06	1,65E-06	2,430E-05	2,799E-05	55,971	4,861E-05	3,6482	75,05
4	2,56	0,544	0,546	3,44E-05	9,65E-06	2,35E-06	2,640E-05	5,438E-05	108,768	5,280E-05	3,6525	69,17
5	2,96	0,628	0,63	3,97E-05	1,11E-05	2,71E-06	3,098E-05	8,537E-05	170,731	6,196E-05	4,1972	67,73
6	4,09	0,647	0,648	5,49E-05	1,14E-05	2,79E-06	4,619E-05	1,316E-04	263,110	9,238E-05	5,3694	58,12
7	4,98	1,08	1,09	6,69E-05	1,91E-05	4,69E-06	5,054E-05	1,821E-04	364,193	1,011E-04	4,6444	45,94
8	5,99	1,69	1,7	8,04E-05	2,99E-05	7,32E-06	5,519E-05	2,373E-04	474,577	1,104E-04	4,604	41,70
9	6,57	5,12	5,13	8,82E-05	9,08E-05	2,21E-05	4,741E-06	2,420E-04	484,058	9,482E-06	0,341	35,96
10	7,03	4,04	4,04	9,46E-05	7,17E-05	1,74E-05	4,487E-05	2,869E-04	573,808	8,975E-05	3,2325	36,01

APPENDIX D

IN THE GROUT PREPARATION

The samples from Kalekim A.Ş. are tested. The change on NO_2 concentration is shown shown in Figure D1 and D2.

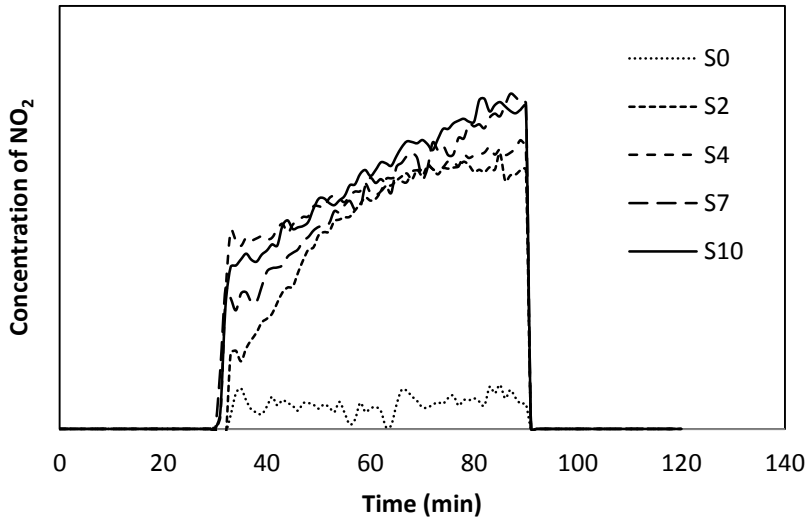

Figure D 1. The effectiveness of in-the-plaster (S) samples with respect to time for NO_2 concentration: total flow rate is 1 l/min, relative humidity is 50%, light intensity is 18.8 W/m^2, inlet NO concentration approximately is 12 ppm.

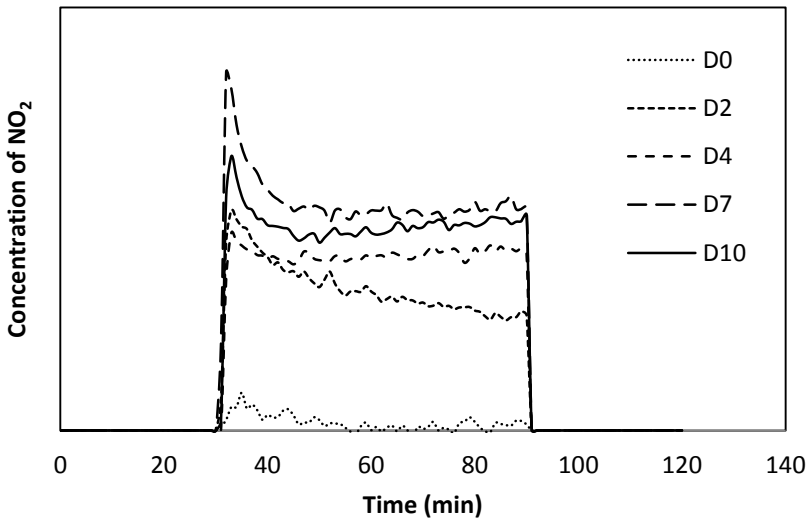

Figure D 2. The effectiveness of in-the-grout (D) samples with respect to time for NO_2 concentration: total flow rate is 1 l/min, relative humidity is 50%, light intensity is 18.8 W/m^2, inlet NO concentration approximately is 12 ppm.